https://doi.org/10.5194/nhess-2020-395
Preprint. Discussion started: 16 December 2020

Natural Hazards and Earth System Sciences
Discussions

Characteristics of building fragility curves for seismic and non-seismic tsunamis: case studies of the 2018 Sunda Strait, 2018 Sulawesi-Palu and 2004 Indian Ocean tsunamis.

Elisa Lahcene[1], Ioanna Ioannou[2], Anawat Suppasri[3], Kwanchai Pakoksung[3], Ryan Paulik[4], Syamsidik Syamsidik[5], Frederic Bouchette[1] and Fumihiko Imamura[3]

[1]GEOSCIENCES-Montpellier, Montpellier University II, France
[2]EPICentre, Department of Civil, Environmental and Geomatic Engineering, University College London, UK
[3]International Research Institute of Disaster Science, Tohoku University, Japan
[4]National Institute of Water and Atmospheric Research (NIWA), Wellington, New Zealand
[5]Tsunami and Disaster Mitigation Research Center (TDMRC), Universitas Syiah Kuala, Banda Aceh, Indonesia

Correspondence to: Elisa Lahcene (elisa.lahcene54@gmail.com), Ioanna Ioannou (ioanna.ioannou@ucl.ac.uk)

Abstract. Indonesia has experienced several recent tsunamis triggered by seismic as well as non-seismic (i.e., landslides) sources. These events damaged or destroyed coastal buildings and infrastructure, and caused considerable loss of life. The impact of tsunami characteristics on structural components can be represented by fragility curves. These cumulative distribution functions express the likelihood of a structure reaching or exceeding a damage state in response to a tsunami hazard intensity measure. Using numerical simulations and post-tsunami observations, we successfully reproduce the hydrodynamic features of the 2018 Sunda Strait and 2018 Sulawesi-Palu tsunamis for the first time. We then compare non-seismic building fragility curves from these events with the ones of the 2004 Indian Ocean tsunami (IOT) to provide a novel understanding of wave period, ground shaking and liquefaction impacts on the structural performance of buildings. Below 5-m flow depth, the 2004 IOT in Khao Lak/Phuket (Thailand), characterized by long wave period due to its seismic source, induces larger damage to buildings than the 2018 Sunda Strait tsunami, triggered by a landslide. We also note that for 4-m flow depth, the building damage probability is almost twice less in Khao Lak/Phuket than in Banda Aceh, where ground motion has been reported before the tsunami arrival. In addition, liquefaction events can cause significant building damage as in Palu, where constructions have been considerably affected by this phenomenon due to the 2018 Sulawesi earthquake. Below 2-m flow depth, the damage probability is greater in Palu than in the Sunda Strait but also in Banda Aceh, although this city has been affected by ground shaking, and then struck by the longer wave period of the IOT.

1. Introduction

Indonesia is regularly facing natural disasters such as earthquakes, volcanic eruptions and tsunamis because of its geographic location in a subduction zone of three tectonic plates (Eurasian, India-Australian and Pacific plates) (Marfai et al., 2008; Sutikno, 2016). The Sunda Arc extends for 6 000 kilometers, from the North of Sumatra to Sumbawa Island (Lauterjung et al., 2010) (Fig. 1a). Megathrust earthquakes regularly occur in this region, causing vertical movement of the ocean floor, which tends to be tsunamigenic (McCloskey et al., 2008; Nalbant et al., 2005; Rastogi, 2007). Those tsunamis are likely to cause greater damage because of prior ground shaking and liquefaction episodes affecting the surrounding areas (Sumer et al., 2007; Sutikno, 2016). They also have longer wave period attacking the coast due to their fault width (Day, 2015; Grezio et al., 2017). On Dec. 26 2004, the Sumatra-Andaman earthquake (M_w= 9.0-9.3) hit the north of Sumatra, Indonesia (Fig. 1b). The rupture of the seafloor is estimated at 1200 km length and around 200 km width (Ammon et al., 2005; Krüger and Ohrnberger,

https://doi.org/10.5194/nhess-2020-395
Preprint. Discussion started: 16 December 2020

Natural Hazards and Earth System Sciences
Discussions

2005; Lay et al., 2005). In the city of Banda Aceh, strong ground shaking were reported (Lavigne et al., 2009). This megathrust earthquake was the second largest ever recorded (wave period ranging from 20 to 50 min) (Løvholt et al., 2006) and caused the deadliest tsunami in the world. Overall, a dozen Asian and African countries have been devastated, with around 280 000 casualties (Asian Disaster Preparedness Center, 2007; Suppasri et al., 2011). Although earthquakes represent the main cause of tsunamis, non-seismic events such as landslides can also initiate one (Grezio et al., 2017; Ward, 2001). After few months of volcanic activity in the Sunda Strait, Indonesia, the Anak Krakatau Volcano finally erupted on Dec. 22 2018, leading to its southwestern flank failure (Fig. 1c). The subaerial/submarine landslide volume ranges from 0.15 to 0.30 km^3 (Grilli et al., 2019; Paris et al., 2020). It triggered a short wave period tsunami (~7 min) (Muhari et al., 2019), which devastated the western coast of Banten and the southern coast of Lampung with a death toll of 437 (Heidarzadeh et al., 2020; Muhari et al., 2019; National Agency for Disaster Management (BNPB), 2018; Syamsidik et al., 2020). Almost two months before this event, an unexpected tsunami struck Palu-Bay, on Sulawesi Island, claiming 2000 deaths and considerable loss property (Association of Southeast Asian Nations (ASEAN)-Coordinating Centre for Humanitarian Assistance on disaster, 2018). The Sulawesi earthquake (M_w= 7.5) occurred along the Palu-Koro strike-slip fault, 50 km northwest of Palu-Bay (Fig. 1d). The ground shaking led to significant liquefaction episodes along the coast (Paulik et al., 2019; Sassa and Takagawa, 2019). The tsunami was not considered destructive due to the fault mechanism. However, the wave height reported to the Pantoloan tidal gauge was largely exceeded. The tsunami rapidly reached Palu (~8 min), implying that its source was inside or near the bay (Muhari et al., 2018; Omira et al., 2019). Its short wave period (~3.5 min) also indicates a non-seismic source such as landslide. So far, the main assumption is that the horizontal displacement of the fault triggered a massive submarine landslide inside Palu-Bay, responsible for the main tsunami. A dozen of coastal landslides were reported during field surveys and likely contributed to amplify tsunami waves (Arikawa et al., 2018; Heidarzadeh et al., 2019; Muhari et al., 2018; Omira et al., 2019; Pakoksung et al., 2019).

Koshimura et al., 2009b suggested the term "tsunami fragility" as a new measure for estimating structural damage and casualties caused by a tsunami. Tsunami fragility curves are cumulative distribution functions expressing the damage probability of structures (or death ratio) based on the hydrodynamic characteristics of the tsunami inundation flow (flow depth, flow velocity and hydrodynamic force) (Koshimura et al., 2009b, 2009a). These functions have been widely developed after tsunami events such as the 2004 Indian Ocean tsunami (Koshimura et al., 2009a, 2009b; Murao and Nakazato, 2010; Suppasri et al., 2011), the 2006 Java tsunami (Reese et al., 2007), the 2010 Chilean tsunami (Mas et al., 2012) or the 2011 Great East Japan tsunami (Suppasri et al., 2012, 2013). Several methods aim to develop building fragility curves based on (i) a statistical analysis of on-site observations during field surveys of damage and flow depth data (empirical methods) (Peiris, 2006; Suppasri et al., 2015, 2020), (ii) the interpretation of damage data from remote sensing coupled with tsunami inundation modelling (hybrid methods) (Koshimura et al., 2009a; Mas et al., 2020; Suppasri et al., 2011) or (iii) structural modelling and response simulations (analytical methods) (Attary et al., 2017; Macabuag et al., 2014).

In this study, building fragility curves of the 2018 Sunda Strait, 2018 Sulawesi-Palu and 2004 IO tsunamis are empirically developed from field survey data. The empirical vulnerability assessment draws on the GEM guidelines (Rossetto et al., 2014). A database has been established for the regions of Sunda Strait by Syamsidik et

https://doi.org/10.5194/nhess-2020-395
Preprint. Discussion started: 16 December 2020

Natural Hazards and Earth System Sciences
Discussions
Open Access
EGU

al., 2019b (DB_Sunda2018), Sulawesi-Palu by Paulik et al., 2019 (DB_Palu2018) and Khao Lak/Phuket by Ruangrassamee et al., 2006 and Foytong and Ruangrassamee, 2007 (DB_Thailand2004). Those databases are treated separately to illustrate the characteristics of the curves for seismic and non-seismic tsunamis. The 2018 Indonesian tsunamis are uncommon events poorly understood compared to earthquake-generated tsunamis. Therefore, to improve our understanding of potential damage caused by the next non-seismic tsunamis along Indonesian coasts, the Sunda Strait and Sulawesi-Palu curves are built from two-layer modelling (TUNAMI 2-layer). In parallel, Koshimura et al., 2009a produced fragility curves in Banda Aceh (Indonesia) from satellite images before and after the 2004 IOT. The seismic curves of the IOT are compared with the non-seismic ones of the 2018 Sunda Strait and Sulawesi-Palu tsunamis. For the first time, the characteristics of building fragility curves according to the wave period, the ground shaking and liquefaction events are exposed. Studying such impacts on the structural performance of buildings improves knowledge on the relationship between local vulnerability and tsunami hazard in Indonesia.

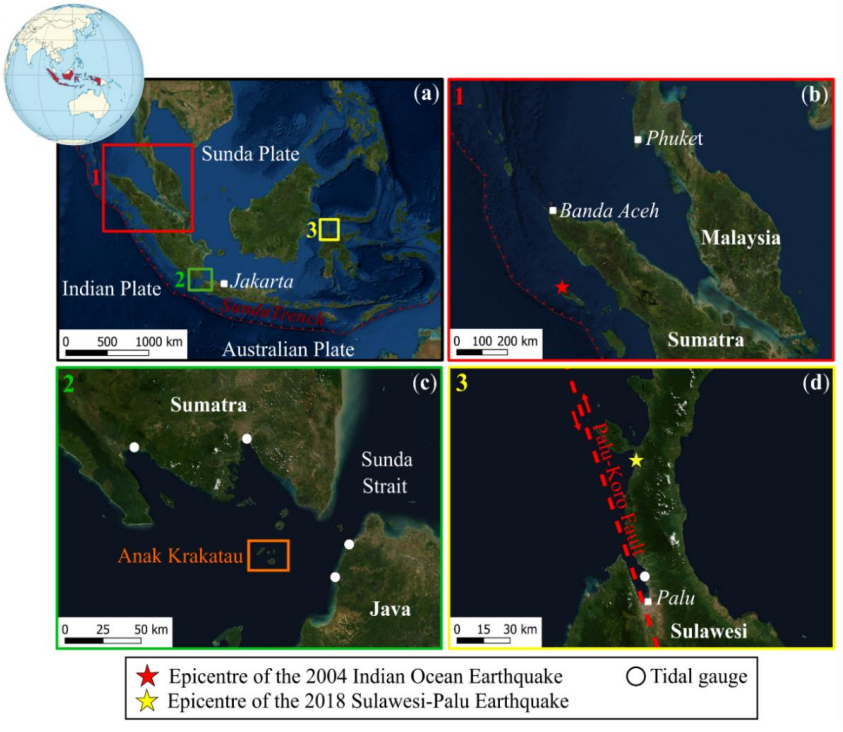

Figure 1. (a) Indonesia partially surrounded by the Sunda Trench, (b) epicenter location of the 2004 Indian Ocean earthquake, (c) location of the Sunda Strait and the Anak Krakatau volcano and (d) epicenter location of the 2018 Palu-Sulawesi earthquake and the Palu-Koro fault crossing Palu-Bay, on Sulawesi Island, Indonesia (background ESRI).

https://doi.org/10.5194/nhess-2020-395
Preprint. Discussion started: 16 December 2020

Natural Hazards and Earth System Sciences
Discussions

2. Post-disaster databases

This study is based on data from numerous field surveys conducted in urban areas strongly affected by the tsunamis. The databases of the 2018 Sunda Strait, 2018 Sulawesi-Palu and 2004 IO (Khao Lak/Phuket, Thailand) events are respectively called DB_Sunda2018 (Syamsidik et al., 2019b), DB_Palu2018 (Paulik et al., 2019) and DB_Thailand2004 (Foytong and Ruangrassamee, 2007; Ruangrassamee et al., 2006). Each database gathers exclusive information regarding the degree of damage, the building characteristics (e.g. construction material type) and the flow depth traces. Overall, DB_Palu2018, DB_Thailand2004 and DB_Sunda2018 include information on 463, 136 and 98 buildings respectively. We consider those databases statistically representative samples of the impact of the wave period, ground shaking and liquefactions on the building damage probability. A brief analysis of the key variables (i.e., damage scale, building class, and tsunami intensity) are presented and the main data deficiencies are highlighted.

2.1. Building characteristics

Each survey recorded the building construction material, which influences the damage probability (Suppasri et al., 2013). With regard to the 98 buildings included in DB_Sunda2018: 70 are confined masonry, 27 are timber and 1 is steel frame building. In DB_Palu2018, most of the buildings are confined masonry with unreinforced clay bricks (~85 %). The database also includes reinforced concrete, timber and steel buildings. Finally, DB_Thailand2004 contains only reinforced concrete buildings.

2.2. Damage states

Each field survey adopted a different scale to record the degree of structural damage. In DB_Sunda2018, the five-state damage scale, proposed by Macabuag et al., 2016 and Suppasri et al., 2020, is adopted, ranging from no damage to complete damage/washed away. In DB_Palu2018, the observed damage was classified into four states: no damage, partial damage repairable, partial damage unrepairable and complete damage, as proposed by Paulik et al., 2019. Finally, in DB_Thailand2004, a four-state damage scale is defined by Ruangrassamee et al., 2006. To simplify the comparison between the fragility curves, a harmonisation of damage scales is proposed (Table 1). In this study, a four-state damage scale ranging from ds_0- ds_3 is used.

Table 1. Harmonization between the different damage scales used in DB_Sunda2018, DB_Palu2018 and DB_Thailand2004.

Damage state	DB_Sunda2018	DB_Palu2018	DB_Thailand2004
ds_0	No damage	No damage	No damage
ds_1	Minor damage Moderate damage	Partial damage, repairable	Damage to secondary members
ds_2	Major damage	Partial damage, unrepairable	Damage to primary members
ds_3	Complete damage, washed away	Complete damage	Collapse

2.3. Tsunami intensity

The tsunami intensity has been measured in terms of flow depth level. In Table 2, the number of flow depth traces at surveyed building and the range of flow depth levels are presented. We note that 19 out of the 136 surveyed

https://doi.org/10.5194/nhess-2020-395
Preprint. Discussion started: 16 December 2020

Natural Hazards and Earth System Sciences
Discussions

buildings do not have a flow depth trace in DB_Thailand2004; the information on these buildings are ignored in the analysis.

Table 2. Observed flow depth traces at buildings and range of flow depth levels in DB_Sunda2018, DB_Palu2018 and DB_Thailand2004.

	DB_Sunda2018	DB_Palu2018	DB_Thailand2004
Observed flow depth traces at building	98	463	117
Range of observed flow depth levels at building (m)	(0.20, 6.60)	(0.10,3.65)	(0.15,10.00)

3. Tsunami intensity simulations

3.1. Tsunami numerical modelling with a landslide source

3.1.1. Tsunami inundation model

The tsunami model TUNAMI two-layer used in Sunda Strait and Palu areas is based on a two-layer numerical model solving non-linear shallow water equations. It considers two-interfacing layers, appropriate kinematic and dynamic boundary conditions at the seafloor, interface, and water surface (Imamura and Imteaz, 1995; Pakoksung et al., 2019). Landslide-generated tsunami is reproduced by modelling interactions between tsunami generation and submarine landslides as upper and lower layers. The mathematical model performed in the landslide-tsunami code is obtained from a stratified medium with two layers. The first layer, composed of a homogeneous inviscid fluid with constant density, ρ_1, represents the seawater, and the second layer is composed of a fluidized granular material with a density, ρ_s, and porosity, φ. As assumed by Macías et al., 2015, the mean density of the fluidized sliding mass is constant and equals $\rho_2 = (1-\varphi)\rho_s + \varphi\rho_1$. The two layers are also considered immiscible. The governing equations are written as follows:

Continuity equation of the seawater (first layer).

$$\frac{\partial Z_1}{\partial t} + \frac{\partial Q_{1x}}{\partial x} + \frac{\partial Q_{1y}}{\partial y} = 0 \quad (1)$$

Momentum equations of the seawater in the x and y directions.

$$\frac{\partial Q_{1x}}{\partial t} + \frac{\partial}{\partial x}\left(\frac{Q_{1x}^2}{D_1}\right) + \frac{\partial}{\partial y}\left(\frac{Q_{1x}Q_{1y}}{D_1}\right) + gD_1\frac{\partial Z_1}{\partial x} + gD_1\frac{\partial Z_2}{\partial x} + \tau_{1x} = 0 \quad (2)$$

$$\frac{\partial Q_{1y}}{\partial t} + \frac{\partial}{\partial x}\left(\frac{Q_{1x}Q_{1y}}{D_1}\right) + \frac{\partial}{\partial y}\left(\frac{Q_{1y}^2}{D_1}\right) + gD_1\frac{\partial Z_1}{\partial y} + gD_1\frac{\partial Z_2}{\partial y} + \tau_{1y} = 0 \quad (3)$$

Continuity equation of the landslide (second layer).

$$\frac{\partial Z_2}{\partial t} + \frac{\partial Q_{2x}}{\partial x} + \frac{\partial Q_{2y}}{\partial y} = 0 \quad (4)$$

Momentum equations of the landslide in the x and y directions.

https://doi.org/10.5194/nhess-2020-395
Preprint. Discussion started: 16 December 2020

Natural Hazards and Earth System Sciences
Discussions

$$\frac{\partial Q_{2x}}{\partial t} + \frac{\partial}{\partial x}\left(\frac{Q_{2x}^2}{D_2}\right) + \frac{\partial}{\partial y}\left(\frac{Q_{2x}Q_{2y}}{D_2}\right) + gD_2\frac{\partial Z_2}{\partial x} + gD_2\frac{\rho_1}{\rho_2}\frac{\partial Z_1}{\partial x} + \tau_{2x} = 0 \quad (5)$$

$$\frac{\partial Q_{2y}}{\partial t} + \frac{\partial}{\partial x}\left(\frac{Q_{2x}Q_{2y}}{D_2}\right) + \frac{\partial}{\partial y}\left(\frac{Q_{2y}^2}{D_2}\right) + gD_2\frac{\partial Z_2}{\partial y} + gD_2\frac{\rho_1}{\rho_2}\frac{\partial Z_1}{\partial y} + \tau_{2y} = 0 \quad (6)$$

Index 1 and 2 refer to the first and the second layers respectively. $Z_i(x,y,t)$, $Q_i(x,y,t)$ and $\tau_i(x,y,t)$ represent the level of the layer based on the mean water level, the vertically integrated discharge and the bottom stress in each layer at each point (x,y) over the time t, respectively. D_i denotes the thickness of each layer. ρ_1 and ρ_2 are the densities of the seawater and the landslide. The tsunami model provides the maximum water flow depth and flow velocity along the coast during the tsunami inundation.

3.1.2 Flow resistance within a tsunami inundation area

In Sunda Strait area, three computational domains are used with a grid size of 20 m while in Palu, one computational domain with the finest grid size of 1 m is defined (Fig. 2a-d). For tsunami inundation modelling in a densely populated area, we apply a resistance law with the composite equivalent roughness coefficient depending on the land use and building conditions, as shown in Eq. (7) (Aburaya and Imamura, 2002; Koshimura et al., 2009a).

$$n = \sqrt{n_0^2 + \frac{C_D}{2gd} * \frac{\theta}{100 - \theta} * D^{4/3}} \quad (7)$$

n_o corresponds to the Manning's roughness coefficient (n_o = 0.025), C_D represents the drag coefficient (C_D = 1.5 (Federal Emergency Management Agency (FEMA), 2003)), d signifies the horizontal scale of buildings (~15 m), D corresponds to the simulated flow depth (m), and θ is the building occupation ratio in the computational grid. In the urban areas of Sunda Strait and Palu, the average occupation ratios are 24 % and 84 % respectively (Fig. 2b,d).

https://doi.org/10.5194/nhess-2020-395
Preprint. Discussion started: 16 December 2020

Natural Hazards and Earth System Sciences
Discussions

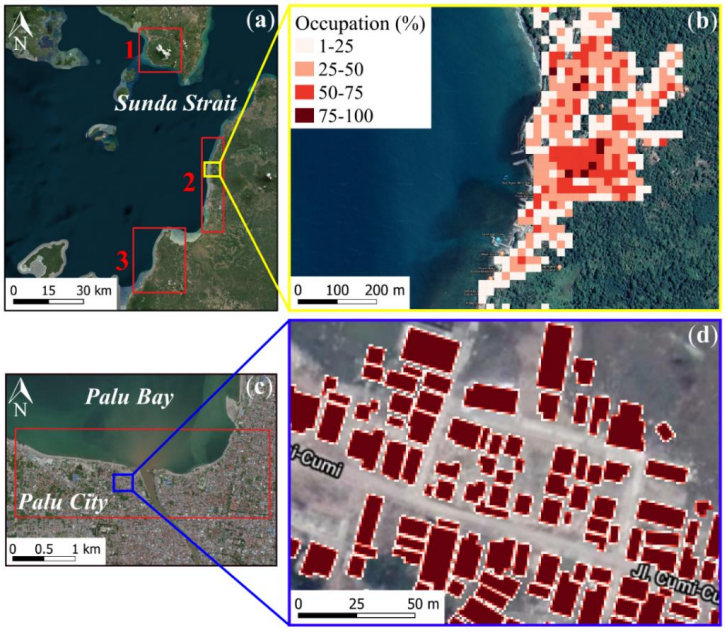

Figure 2. (a,c) Computational areas in the Sunda Strait (regions 1-3) and Palu-City, (b,d) magnified view of the building occupation ratio in region 2 of the Sunda Strait (20-m resolution) and Palu-City (1-m resolution) (background ESRI and © Google Maps).

3.2. Calibration and validation of the tsunami inundation model

3.2.1. Performance parameters

The tsunami inundation model is calibrated using two performances parameters: K (or μ) and κ (or σ) proposed by AIDA, 1978, as defined below:

$$\log K = \frac{1}{n}\sum_{i=1}^{n} \log K_i \tag{8}$$

$$\log \kappa = \sqrt{\frac{1}{n}\sum_{i=1}^{n} (\log K_i)^2 - (\log K)^2} \tag{9}$$

$$K_i = \frac{x_i}{y_i} \tag{10}$$

x_i and y_i are the recorded and simulated tsunami flow depths at location i. K is defined as the geometrical mean of K_i and κ is defined as deviation/variance from K. The Japan Society of Civil Engineers (JSCE), 2002 recommends $0.95 < K < 1.05$ and $\kappa < 1.45$ for the model results to achieve "good agreement" in the tsunami source model and propagation/inundation model evaluation (Otake et al., 2020; Pakoksung et al., 2018).

https://doi.org/10.5194/nhess-2020-395
Preprint. Discussion started: 16 December 2020

Natural Hazards and Earth System Sciences
Discussions

3.2.2. The 2018 Sunda Strait tsunami inundation model

The 2018 Sunda Strait tsunami simulations are based on the density of the landslide (ρ_2), its stable slope (α), its volume (V_L) and its sliding time (t_S). The Manning's roughness coefficients inland and on the seafloor are set to 0.03 and 0.025 respectively, which are typical values for vegetated and shallow water areas (Kotani, 1998). As proposed by Paris et al., 2020, the low sensitivity parameters are set as follows: ρ_2 = 1500 kg/m^3, α = 5° and V_S = 0.15 km^3. The best fit between the simulated and observed flow depths at buildings is reached for 10 min sliding time. DB_Sunda2018 includes 98 observed flow depths. However, only 94 traces are overlaid by the simulated tsunami inundation zone. Most of these simulated flow depths are underestimated compared to the observed ones, with a mean difference of 0.28 m. The Digital Surface Model (DSM) has been automatically corrected to remove the effects of vegetation and buildings. The resulting Digital Elevation Model (DEM) is corrected once again to improve the topography reliability at buildings. The different corrections applied to the topography are displayed in Fig. 3. Some profiles are realized along the Sunda Strait coasts to illustrate the modifications applied to the initial DSM (Fig. 4). K and κ values for damaged buildings are 0.99 and 1.11, respectively, which means that "good agreement" is achieved for the Sunda Strait tsunami model, displayed in Fig. 5.

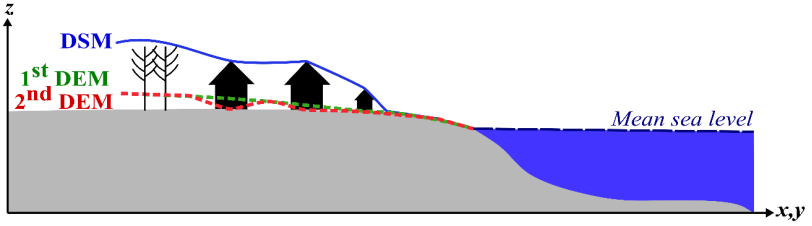

Figure 3. Topographic corrections performed on the Digital Surface Model (DSM) and the Digital Elevation Model (1st DEM); the final Digital Elevation Model is used as new topography in TUNAMI 2-layer model.

https://doi.org/10.5194/nhess-2020-395
Preprint. Discussion started: 16 December 2020

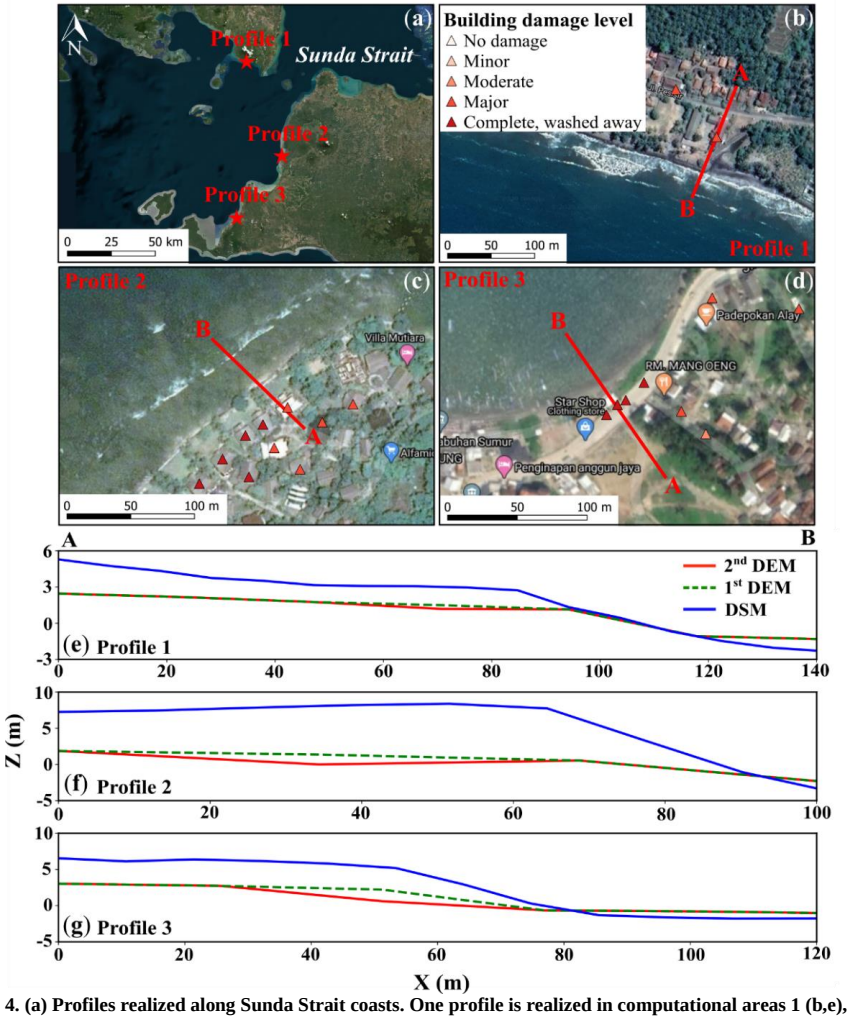

Figure 4. (a) Profiles realized along Sunda Strait coasts. One profile is realized in computational areas 1 (b,e), 2 (c,f) and 3 (d,g) to illustrate the topographic corrections applied to the Digital Surface Model (DSM) (background ESRI and © Google Maps).

https://doi.org/10.5194/nhess-2020-395
Preprint. Discussion started: 16 December 2020

Natural Hazards and Earth System Sciences
Discussions
Open Access
EGU

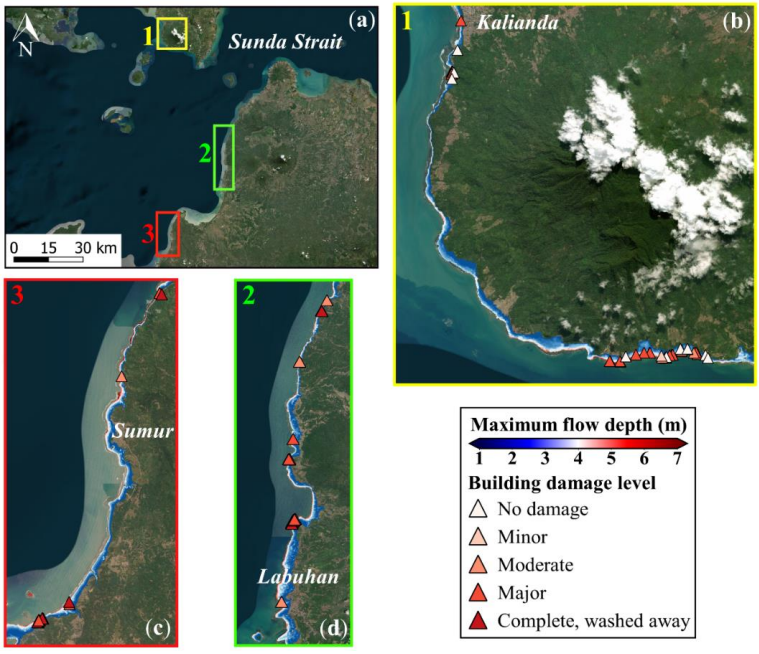

Figure 5. Sunda Strait final tsunami inundation model with the maximum simulated flow depth overlaying on the damaged building data for computational areas 1 (a,b), 2 (a,c) and 3 (a,d) (background ESRI).

205

3.2.3. The 2018 Sulawesi-Palu tsunami inundation model

The 2018 Palu tsunami simulations are based on fourteen landslides, which can be separated into two classes: large (L) and small (S). The hypothesized location of large landslides is our main assumption while small landslides location stands on observations from satellite imagery and video footage (Carvajal et al., 2019) (Fig. 6, Table 3).
210 The simulated wave height at the Pantoloan tidal gauge reproduces well the observations (Fig. 7). The calibration of the model is based on the landslide S8 because (i) as small landslide, its volume is too small to distort the simulated wave height at the Pantoloan tidal gauge, (ii) it has the largest volume among the other small landslides and (iii) it is close and ideally oriented to Palu-City. The density of the landslides (ρ_2), their stable slope (α), their sliding time (t_s) are set as follows: $\rho_2 = 2000$ kg/m^3 (Palu bay receives a large amount of fine continental deposits
215 such as clay-sized sediments (Frederik et al., 2019)), $\alpha = 14°$ (Chakrabarti, 2005) and $t_S = 10$ min. For a landslide ratio of 1.2, the tsunami model shows a great similarity between observed and simulated flow depths (a = 1.027). DB_Palu2018 includes 463 observed flow depths. Nevertheless, only 175 traces are overlaid by the simulated tsunami inundation zone, depicted in Fig. 8. The geometric mean is near the recommended values ($K = 0.93$) while the standard deviation as well as the Root Mean Square Error (RMSE) are high ($\kappa = 2.18$, RMSE = 0.92 m).
220 Therefore, we propose to study three confidence intervals of 1.5, 1 and 0.5 m, which corresponds respectively to 153, 124 and 75 out of 175 flow depths traces at building. First, the 1.5 and 1 m confidence intervals represent samples sufficiently large to illustrate the main trend of the original dataset. Then, the similarity between observed and simulated flow depths included in the 1 m confidence interval is higher than the flow depths comprised in the 1.5 m one. Therefore, we consider the 1 m confidence interval more prone to develop reliable fragility curves (Fig.
225 9); K and κ values for damaged buildings are 0.93 and 2.14 respectively, with a Root Mean Square Error of 0.26

https://doi.org/10.5194/nhess-2020-395
Preprint. Discussion started: 16 December 2020

Natural Hazards and Earth System Sciences
Discussions

m. The validity of the model is mainly based on the geometric mean *K*, close to 0.95, so we consider the tsunami inundation model accurate enough (Fig. 8).

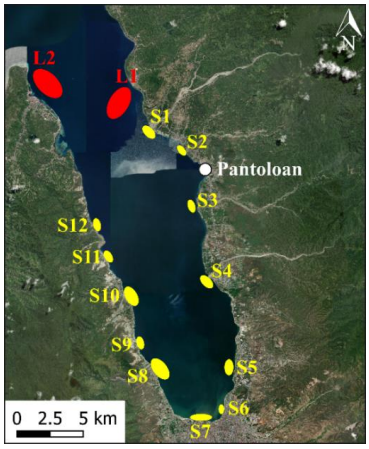

230 **Figure 6. Location of the hypothesized landslides (S: small and L: large) in Palu-Bay (background ESRI).**

Table 3. Hypothesized landslide parameters (location and volume) in Palu-Bay.

No.	Location (latitude; longitude)	Volume (10^6 m^3)
L1	-0.655;119.749	37.54
L2	-0.670;119.801	31.93
S1	-0.680;119.821	0.60
S2	-0.703;119.842	0.18
S3	-0.737;119.851	0.25
S4	-0.789;119.862	0.75
S5	-0.852;119.878	0.22
S6	-0.879;119.871	0.60
S7	-0.885;119.858	2.44
S8	-0.846;119.822	4.45
S9	-0.832;119.813	0.83
S10	-0.804;119.808	2.17
S11	-0.774;119.792	0.55
S12	-0.754;119.788	0.83

https://doi.org/10.5194/nhess-2020-395
Preprint. Discussion started: 16 December 2020

Natural Hazards and Earth System Sciences
Discussions

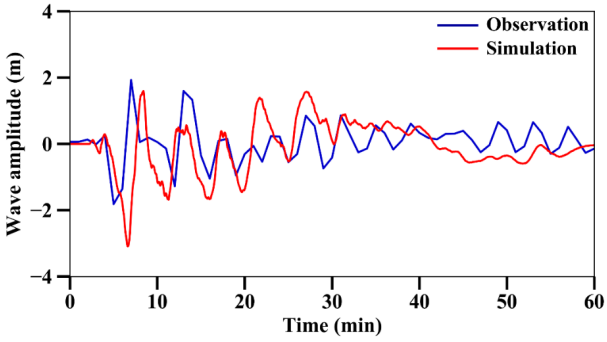

Figure 7. Comparison between observed (blue) and simulated (red) wave heights at Pantoloan tidal gauge, in Palu-Bay, Sulawesi, Indonesia.

Figure 8. Sulawesi-Palu final tsunami inundation model with the maximum simulated flow depth overlaying on the damaged building data (background ESRI).

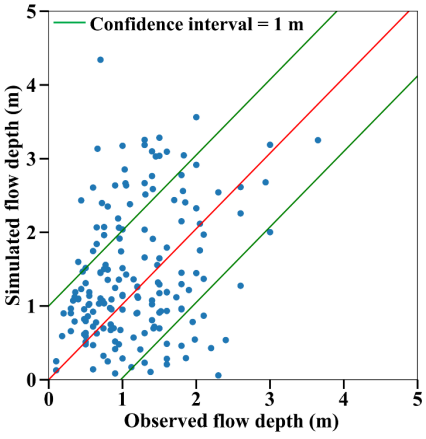

Figgure 9. Comparison between observed and simulated flow depths at damaged building for a S8 ratio of 1.2; a confidence interval is set at 1-m flow depth.

4. Tsunami fragility assessment

235 The fragility of the damaged buildings is empirically assessed for the three databases. In DB_Sunda2018 and DB_Palu2018, we select the buildings having both observed and simulated values of flow depth (Table 4). For instance, among the 98 buildings of DB_Sunda2018, 67 confined masonry, 26 timber and 1 steel buildings have

https://doi.org/10.5194/nhess-2020-395
Preprint. Discussion started: 16 December 2020


Natural Hazards and Earth System Sciences
Discussions

both flow depths values. We thus define a new database called DB_Sunda2018'. DB_Palu2018' includes 119 confined masonry, 4 reinforced concrete and 1 timber buildings. The development of the computed fragility curves for the 2018 Sunda Strait and 2018 Sulawesi-Palu tsunamis is directly based on DB_Sunda2018' and DB_Palu2018'.

Table 4. Total number of buildings having both an observed and a simulated tsunami intensity measures in the Sunda Strait and Palu areas.

Database	Tsunami intensity measure			
	Observed flow depth*	Simulated flow depth	Simulated flow velocity	Simulated hydrodynamic force
DB_Sunda2018'	94 out of 98	94	94	94
DB_Palu2018'	124 out of 463	124	124	124

*surveyed buildings included in the simulated tsunami inundation zone.

4.1. Exploratory analysis

Prior to selecting a statistical model, an exploratory analysis is carried out to assess the trends that the available data follow and to determine the main important explanatory variables that need to be included in the statistical model and their influence on the slope and intercept of the fragility curves. The relationship between the tsunami intensity with the probability of damage can be explored by fitting a Generalised Linear Model (GLM), which is proposed by the Global Earthquake Model (GEM) Guidelines (Rossetto et al., 2014), to the data of each database. A GLM assumes that the response variable y_{ij} is assigned 1 if the building j sustained damage $DS \geq ds_i$ and 0 otherwise. The variable follows a Bernoulli distribution:

$$y_{ij} \sim Bernoulli\ (\pi_i(\tilde{x}_j)) \tag{11}$$

where $\pi_i(\tilde{x}_j)$ is the probability that a building j will reach or exceed the 'true' damage state ds_i given estimated tsunami intensity level $\tilde{x}_j$. The Bernoulli distribution is characterised by its mean:

$$\mu_{ij} = \pi_i(\tilde{x}_j) \tag{12}$$

which is expressed here in terms of a probit model defined in terms of Φ[.], the cumulative distribution function of a standard normal distribution:

$$\Phi^{-1}[\pi_i(\tilde{x}_j)] = \eta_{ij} \tag{13}$$

where η_{ij} is the linear predictor, which can be written in the form:

$$\eta_{ij} = \theta_{0i} + \theta_{1i} \ln(\tilde{x}_j) \tag{14}$$

https://doi.org/10.5194/nhess-2020-395
Preprint. Discussion started: 16 December 2020


Natural Hazards and Earth System Sciences
Discussions
Open Access
EGU

Where θ_{1i}, θ_{0i} are the two regression coefficients, representing the slope and the intercept, respectively, of the fragility curve corresponding to damage state ds_i. For the exploratory analysis, the tsunami intensity is measured in terms of observed flow depth levels. GLM models are also fitted to subsets of data of each database in order to explore the importance of the construction material to the shape of the fragility curves.

4.1.1. DB_Sunda2018'

The GLM models are fitted to the data in DB_Sunda2018' (irrespective of their structural characteristics). The obtained probit functions are plotted against the natural logarithm of the observed flow depth in Fig. 10a in order to explore how the slope and the intercept of the models change for each damage state. The 90 % confidence intervals around the best-estimate curves are also included. All three curves have positive slopes, which indicates that the flow depth is an adequate descriptor of the damage caused by a tsunami as the probability of a given damage state being reached or exceeded increases with the increase in the flow depth. Moreover, the slope of each function appears to be similar for ds_2 and ds_3 and different for ds_1. Nonetheless, the curve corresponding to ds_1 is also associated with substantial uncertainty. In Figure 10b, probit models are also fitted to subsets of the available data for the two main construction materials. It should be mentioned that one of the drawback of the small database is that not all damage states have been observed for each building class. Therefore, the comparison of the probit models is limited for damage states ds_2 and ds_3. The intercept of the curves for the two material types appear be sustainably different. As expected, the timber buildings appear to be the more vulnerable than the confined masonry buildings. The difference can be attributed mainly to their intercept as the two curves appear to be parallel. This indicates the need to develop a statistical model, which allows only for the intercept to change with the construction material.

https://doi.org/10.5194/nhess-2020-395
Preprint. Discussion started: 16 December 2020

Natural Hazards and Earth System Sciences
Discussions
Open Access
EGU

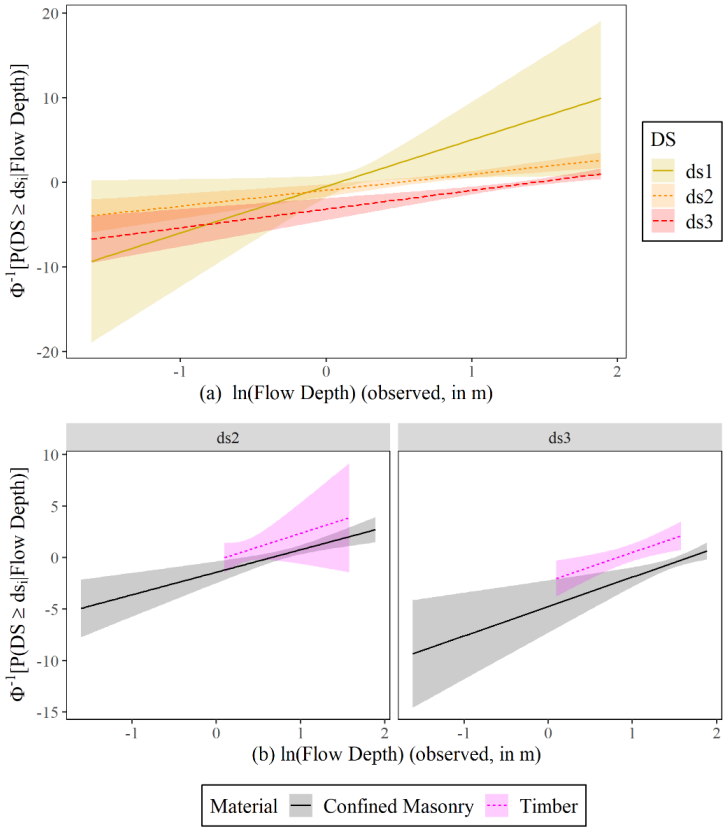

Figure 10. Probit functions fitted for each individual damage state to (a) DB_Sunda2018' in order to assess whether the observed flow depth is an efficient descriptor of damage; (b) to assess whether the construction material affected the shape of fragility curves for ds_2 and ds_3. In both cases, the 90 % confidence interval is plotted.

290

4.1.2. DB_Palu2018'

GLM models are also fitted to the data in DB_Palu2018' using the observed tsunami flow depth to express the tsunami intensity in order to construct fragility curves and their 90 % confidence intervals for the three individual damage states, as depicted in Fig. 11a. The data seems to produce fragility curves with positive slopes for d_{S1} and
295 d_{S2} and a negative slope for d_{S3}. This latter observation is counter-intuitive as it is expected the likelihood of collapse to grow with the increase of the tsunami depth. This outcome could be attributed to the collected sample, which includes very few collapsed buildings observed at low flow depth levels. In Figure 11b, fragility curves for individual damage states and for masonry and reinforced concrete buildings, which have the two larger sample sizes in this database, are also depicted. The confidence intervals of the curves corresponding to reinforced
300 concrete buildings appear to be significantly wider due to the very small sample size and overlap with their counterparts for confined masonry buildings. It indicates that fragility curves specific for given material types are not feasible due to the very small sample of the reinforced concrete buildings.

https://doi.org/10.5194/nhess-2020-395
Preprint. Discussion started: 16 December 2020

Natural Hazards and Earth System Sciences
Discussions
Open Access
EGU

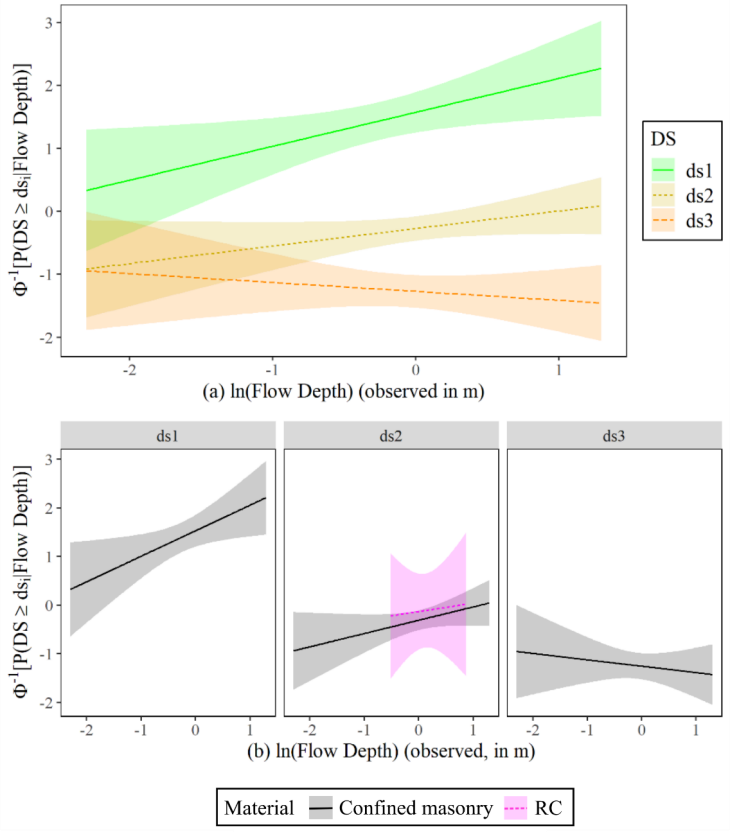

Figure 11. Probit functions fitted for each individual damage state to (a) DB_Palu2018' in order to assess whether the observed flow depth is an efficient descriptor of damage; (b) to assess whether the construction material affected the shape of fragility curves for ds_1, ds_2 and ds_3 (RC: Reinforced concrete). In both cases, the 90 % confidence interval are plotted.

4.1.3. DB_Thailand2004

305 GLM models are finally fitted to DB_Thailand2004 in order to construct fragility curves and their 90 % confidence intervals for the three individual damage states, as depicted in Fig. 12. The data seem to produce fragility curves with positive slopes for all three damage states and also appear to be parallel to each other.

https://doi.org/10.5194/nhess-2020-395
Preprint. Discussion started: 16 December 2020

Natural Hazards and Earth System Sciences
Discussions

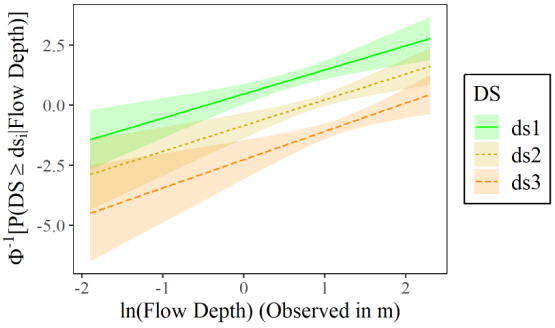

Figure 12. Probit functions fitted for each individual damage state to DB_Thailand2004 in order to assess whether the observed flow depth is an efficient descriptor of damage. The 90 % confidence interval are plotted.

4.2. Statistical model selection

Parametric statistical models for the three databases are constructed based on the aforementioned observations. This section aims to (i) to identify the simulated tsunami measure type which fits the data best and (ii) to construct fragility curves for the tsunami intensity type that fits the data best.

Ideally, the response variable y_{ij} of an appropriate statistical model is the damage state $i = \{0, 1, 2, 3\}$ sustained by a building j. The damage state follows a categorical distribution (i.e. also called a generalized Bernoulli distribution) which describes the possible levels of damage $i = \{0, 1, 2, 3\}$ sustained by a given building (Table 1). The random component of this model can be written as:

$$y_{ij} \sim Categorical\ (P(DS = ds_i|\tilde{x}_j)) \tag{15}$$

where $P(DS = ds_i|\tilde{x}_j)$ is the probability that a building j will reach the 'true' damage state ds_i given estimated tsunami intensity level $\tilde{x}_j$:

$$P(DS = ds_i|\tilde{x}_j) = \begin{cases} 1 - \pi_i(\tilde{x}_j), & i = 0 \\ \pi_i(\tilde{x}_j) - \pi_{i+1}(\tilde{x}_j), & 0 < i < i_{max} \\ \pi_i(\tilde{x}_j), & i = i_{max} \end{cases} \tag{16}$$

The systematic component is determined as:

$$\Phi^{-1}[\pi_i(\tilde{x}_j)] = \eta_{ij} \tag{17}$$

The linear predictor can be expressed in various forms of increasing complexity as depicted in Eq.(18):

$$\eta_{ij} = \begin{cases} \theta_0 + \theta_1\tilde{x}_j & .1 \\ \theta_0 + \theta_{1i}\tilde{x}_j & .2 \\ \theta_0 + \theta_1\tilde{x}_j + \theta_2 class & .3 \\ \theta_0 + \theta_{1i}\tilde{x}_j + \theta_2 class & .4 \\ \theta_0 + \theta_1\tilde{x}_j + \theta_2 class + \theta_3\tilde{x}_j class & .5 \end{cases} \tag{18}$$

https://doi.org/10.5194/nhess-2020-395
Preprint. Discussion started: 16 December 2020

Natural Hazards and Earth System Sciences
Discussions

where *class* is a categorical unordered variable which expresses here the construction material; and $\theta_{0\text{-}3}$ are the unknown regression coefficients of the model. The first two equations (i.e. Eq.(18.1) and Eq.(18.2)) assume that the fragility curves are only influenced by the tsunami intensity. Eq.(18.1) assumes that the slope of the fragility curves is the same for all damage states. By contrast, Eq.(8.2) allows the slope of each curve to vary for each damage state; the slope varies for each fragility curve. The following three equations account for the influence of the building class (i.e. the construction material) in the shape of the fragility curves. All three equations assume that the construction material affects the intercept of the fragility curves and only Eq.(18.5) assumes that the construction material affects both the intercept and the slope of the curves. Finally, Eq.(18.3) and Eq.(18.5) assume identical slope for all fragility curves irrespective of the damage state. By contrast, the Eq.(18.4) relaxes this assumption and considers that the slope changes for each damage state. The combinations of random and systematic components results in five distinct models, as depicted in Table 5. Based on the observations from the exploratory analysis, suitable models are selected for each database and their goodness of fit is assessed. It should be noted that apart from the best estimate fragility curve, its corresponding 90 % confidence intervals are also constructed using bootstrap analysis. According to the latter analysis 1,000 samples of the database are obtained with replacement and the selected model is refitted to the each sample.

Table 5. Statistical models examined for each database.

Model	Component	
	Random	Systematic
M1	Eq.(15)	Eq.(18.1)
M2		Eq.(18.2)
M3		Eq.(18.3)
M4		Eq.(18.4)
M5		Eq.(18.5)

In what follows, multiple models are fitted to each database based on the observations of the exploratory analysis. The goodness of fit of these models for a given tsunami intensity measure is examined with two formal tests as proposed in the GEM guidelines. Firstly, the AIC values estimated for the examined models are estimated and compared. The model with the lowest value fits the data best. Secondly, a series of likelihood ratio tests are performed in order to examine whether the fit provided by the model with the lowest AIC value is statistically significant over alternative models which relaxes its assumptions. It should be noted that apart from the flow depth determined by field observations, the tsunami intensity is also expressed in terms of simulated flow depth, velocity and hydrodynamic force (hydrodynamic features). The AIC value is, also, used to determine which of these simulated intensity measures fits the data best.

4.2.1. DB_Sunda2018'

Following the main observations of the exploratory analysis in Sect. 4.1.1, M3 is considered an acceptable model which considers two explanatory variables: the tsunami intensity and the construction material. To assess its goodness of fit, three alternatives are considered (i.e., M4, M5 and M1) which relax some of its assumptions.

https://doi.org/10.5194/nhess-2020-395
Preprint. Discussion started: 16 December 2020

Table 6. AIC values for the three models fitted to the observed and simulated tsunami intensity measures of DB_Sunda2018'.

Model	AIC			
	Observed flow depth	Simulated flow depth	Simulated flow velocity	Simulated hydrodynamic force
M3	**121**	**129**	**215**	186
M4	125	135	214	**184**
M5	123	131	216	187
M1	152	160	237	208

The fit of the different models for the observed flow depth levels is assessed by comparing their corresponding AIC values, presented in Table 6. M3 has the smallest AIC value than its alternatives, which indicates that it fits the data better than the remaining three models. Nonetheless, some of these differences are rather small and this raises the question of whether the improvement in the fit provided by M3 is statistically significant over its alternatives. To address this, likelihood ratio tests are performed and the results are reported in Table 7. It can be noted that the *p*-values vary for the three comparisons. The *p*-value is significantly above the 0.05 threshold when the identical slope for each fragility curve assumption (i.e. comparison of 'M3' and 'M4') is tested. This means that the M4 (which assumes varying slopes for each damage state) does not provide a statistically significant improvement than its alternative. Therefore, the fit of M3 is the best. Similarly, the *p*-value is well-above the threshold for M3 vs M5, highlighting that the construction material does not affect the slope of the fragility curves. By contrast, the *p*-value is well below the threshold for the comparison of M3 and M1, indicating that the construction material is an important variable and affects only the intercept. Having concluded that M3 based on the observed flow depth data fits the data better than its alternatives (i.e. M4, M5 and M1), the procedure is repeated in order to identify which simulated intensity type fits the data best. In Table 6, the comparison of the AIC values for the three simulated tsunami intensity types are compared. For the simulated flow depth and velocity, M3 is identified as the model which fits the data better than its alternatives and this conclusion is further reinforced by the likelihood ratio tests presented in Table 7. By contrast, model M4 is found to have the smallest AIC value for the simulated hydrodynamic force. Nonetheless, in Table 7, the *p*-value is just above the 5 % threshold which indicates that there is not enough evidence to justify that its fit is statistically significant over M3. Therefore, in this case as well M3 can be considered as the best fitted model. By comparing the AIC values for M3 for all three simulated intensity types, it can be noted that the simulated flow depth is the tsunami intensity which fits the data best. The regression coefficients of the 2018 Sunda Strait fragility curves are depicted in Table A1 (Appendix).

An advantage of constructing a complex model which accounts for the ordinal nature of the damage and for the two main construction materials in the systematic component is that fragility curves for timber buildings can be obtained even for the states for which there are available data. A timber building is found to sustain more damage than a confined masonry one for all damage states. Nonetheless, there is substantial more uncertainty in the prediction of the likelihood of damage and this can be attributed to the rather small sample size.

https://doi.org/10.5194/nhess-2020-395
Preprint. Discussion started: 16 December 2020

Natural Hazards and Earth System Sciences
Discussions

Table 7. Likelihood ratio tests summary for all available observed and simulated tsunami intensity measures of DB_Sunda2018'.

Model	*p*-value			
	Observed flow depth	Simulated flow depth	Simulated flow velocity	Simulated hydrodynamic force
M3 / **M4**	~0.41	~0.72	~0.08	~0.05
M3 / **M5**	~0.56	~0.39	~0.36	~0.35
M3 / **M1**	~0.00	~0.00	~0.00	~0.00

4.2.2. DB_Palu2018'

In Section 4.1.2, the exploratory analysis showed that there is not enough data to allow the differentiation of the fragility curves according to the construction material. It also showed counterintuitive negative slopes for the curves corresponding to the collapse damage state ds_3. To tackle this issue, identical curves are used for the fragility curves for all three damage states (ds_1-ds_3). Therefore, model M1 is fitted to DB_Palu2018' assuming that the tsunami intensity is expressed in terms of simulated flow depth, flow velocity and hydrodynamic force and the AIC values for each model are depicted in Table 8. It can be seen that for all cases the flow depth fits the data the best. The regression coefficients of the 2018 Sulawesi-Palu fragility curves are depicted in Table A2 (Appendix).

Table 8. AIC values for model M1 fitted to the simulated tsunami intensity measures of DB_Palu2018'.

Model	AIC		
	Simulated flow depth	Simulated flow velocity	Simulated hydrodynamic force
M1	276.8	286.3	283.3

4.2.3. DB_Thailand2004

DB_Thailand2004 includes only observations on reinforced concrete buildings. For this database, the exploratory analysis, conducted in Sect. 4.1.3, showed that the slope is identical for the curves corresponding to the three damage states. For this reason model M1 is deemed suitable. To test its goodness of fit, model M2, which relaxes this assumption is also fitted to the data and the comparison of the AIC values is depicted in Table 9. M1 has the smallest AIC value than its alternative, which indicates that the model with identical slopes for the three fragility curves fits the data better than M2 relaxing this assumption. A likelihood ratio test is also performed in order to confirm that the improvement in the fit provided by the more complex M2 model over M1 is not statistically significant. The *p*-value is found to be equal to 0.76, which is significantly above the 0.05 threshold. This suggests that M2 does not provide a statistically better fit to the data, therefore the less complex M1 model fits the data best. The regression coefficients of the 2004 IO (Thailand) fragility curves can be found in Table A3 (Appendix).

Table 9. AIC values for the two models fitted to the observed flow depth of DB_Thailand2004.

Model	AIC

https://doi.org/10.5194/nhess-2020-395
Preprint. Discussion started: 16 December 2020

Natural Hazards and Earth System Sciences
Discussions

	Observed flow depth
M1	164
M2	168

5. Results

5.1 Building fragility curves of the 2018 Sunda Strait tsunami

The fragility curves determine conditional damage probabilities according to the hydrodynamic features (or tsunami intensity) of the 2018 Sunda Strait event for both confined masonry concrete (Fig. 13a-d) and timber (Fig. 14a-d) buildings in DB_Sunda2018'. The curves as functions of the observed flow depths recorded during field surveys by Syamsidik et al., 2019b (Fig. 13,Fig. 14a) reveal a great similarity with the ones based on the simulated flow depths from TUNAMI 2-layer model (Imamura, 1996; Pakoksung et al., 2019) (Fig. 13,Fig. 14b). For instance, when the observed and simulated flow depths reach 3 m, around 99 % of confined-masonry-type buildings sustain minor/moderate damage (ds_{1+2}), 85 % sustain major damage (ds_3) and less than 10 % are completely damaged (ds_4) (Fig. 13a,b). For timber buildings, 99 % sustain minor/moderate, major damage and 70 % are fully devastated (Fig. 14a,b). Consequently, the tsunami functions based on observation and simulation are highly similar, which illustrates the accuracy and the reliability of the tsunami inundation model. For this reason, we consider the curves as functions of the maximum simulated flow velocity (Fig. 13, Fig. 14c) and hydrodynamic force (Fig. 13, Fig. 14d) trustworthy. In Table 10, the building damage probabilities are summarized for 3 m flow depth, 3 m/s flow velocity and 30 kN/m hydrodynamic force. The curves suggest that confined masonry-type buildings have higher performance than timber structures. Most confined masonry and timber buildings collapse when the flow depth is greater than 5 and 2.5 m respectively. When the flow velocity is ranging from 0 to 6 m/s, the majority of confined masonry structures resist to complete damage while most of timber houses are washed away for 1 m/s flow velocity only. Moreover, over half of timber houses collapse beyond 5 kN/m whereas most confined masonry buildings are resilient until 40 kN/m hydrodynamic force.

Here, we compare the completely damaged/washed away fragility curve for confined-masonry buildings to Syamsidik et al., 2020, who developed the curve as a function of observed flow depth for these buildings, as depicted in Fig. 13a. Fragility curves representing complete damage/washed away (ds_4) are similar up to 4-m flow depth. Each curve estimates a 15 % building damage probability at 3.5-m flow depth. However, few data points are available beyond 4.5 m in Sunda Strait area. Therefore, the damage probability uncertainty is greater upon this value, hence the difference between our ds_4-curve and the one produced by Syamsidik et al., 2020.

https://doi.org/10.5194/nhess-2020-395
Preprint. Discussion started: 16 December 2020

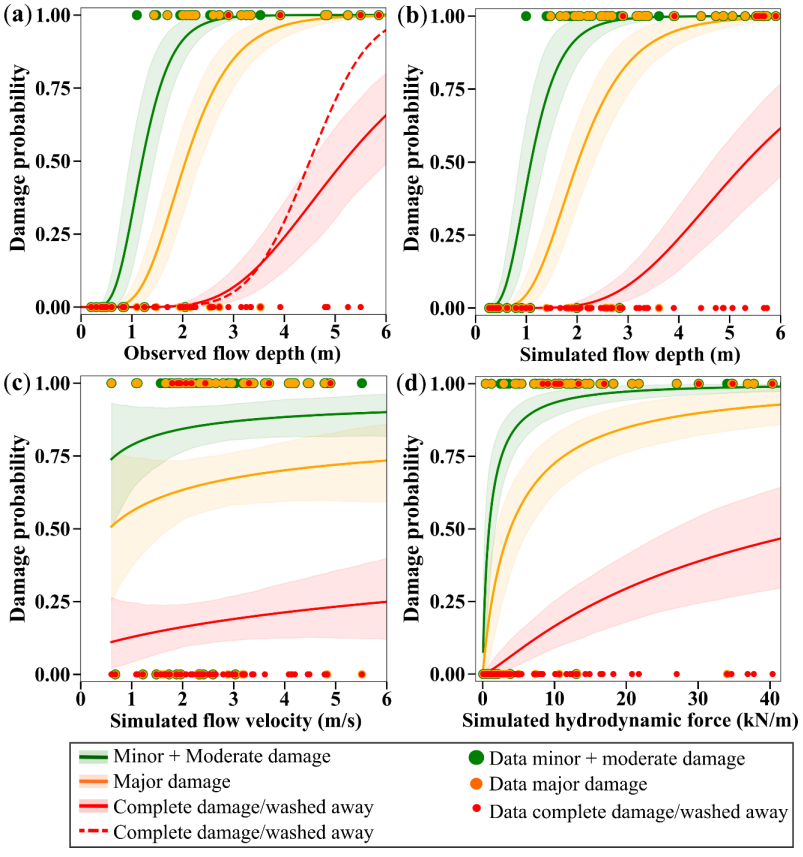

Figure 13. Best-estimate fragility curves as functions of (a) the observed flow depth, produced by Syamsidik et al., 2020 for complete damage/washed away (ds_3, dashed red line), (b) the maximum simulated flow depth, (c) the maximum simulated flow velocity and (d) the simulated hydrodynamic force. The curves are built with their 90 % confidence intervals for confined masonry concrete buildings of DB_Sunda2018' sustaining minor/moderate damage (ds_1, green), major damage (ds_2, orange) and complete damage/washed away (ds_3, red) in the Sunda Strait.

https://doi.org/10.5194/nhess-2020-395
Preprint. Discussion started: 16 December 2020

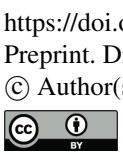

Natural Hazards and Earth System Sciences
Discussions

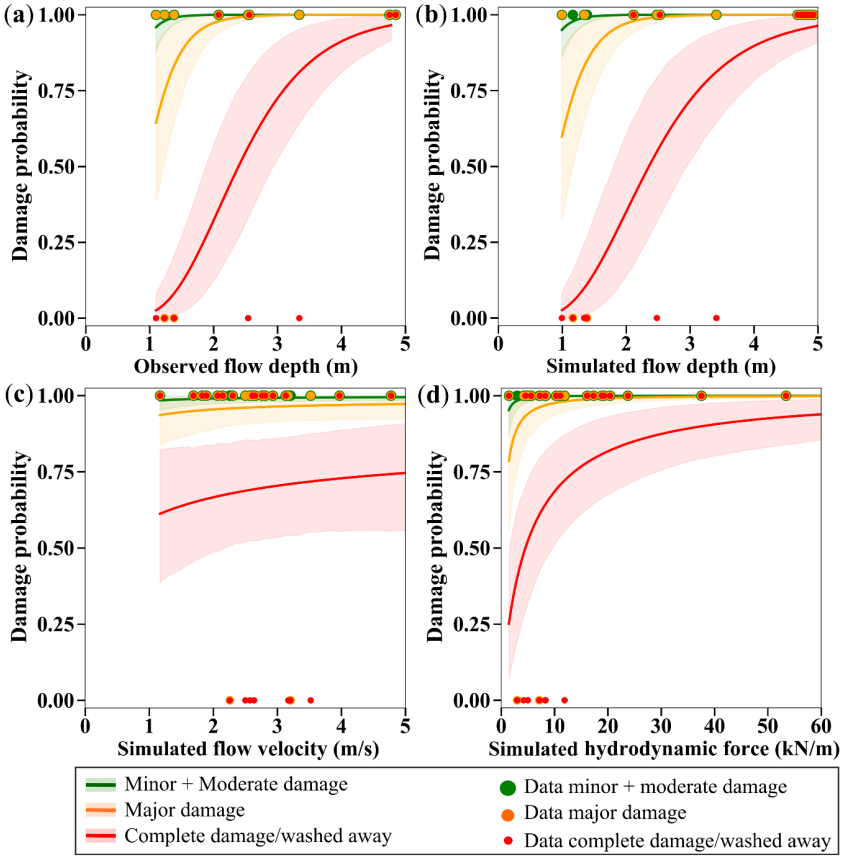

Figure 14. Best-estimate fragility curves, with their 90 % confidence intervals, as functions of (a) the observed flow depth, (b) the maximum simulated flow depth, (c) the maximum simulated flow velocity and (d) the simulated hydrodynamic force for timber buildings of DB_Sunda2018' sustaining minor/moderate damage (ds_1, green), major damage (ds_2, orange) and complete damage/washed away (ds_3, red) in the Sunda Strait.

450 **Table 10. Damage probabilities (ds_{1-3}) when the simulated flow depth, flow velocity and hydrodynamic force reach 3 m, 3 m/s and 30 kN/m respectively for confined masonry concrete (Fig. 13b-d) and timber (Fig. 14b-d) buildings of DB_Sunda2018'.**

Damage state	Tsunami intensity measure	Building damage probability (%)	
		Confined masonry	Timber
Minor/moderate (ds_1)	3 m	99	99
	3 m/s	87	99
	30 kN/m	98	99
Major (ds_3)	3 m	85	99
	3 m/s	67	96
	30 kN/m	89	99
Complete (ds_4)	3 m	9	72

https://doi.org/10.5194/nhess-2020-395
Preprint. Discussion started: 16 December 2020

Natural Hazards and Earth System Sciences
Discussions

	3 m/s	19	70
	30 kN/m	39	88

5.2 Building fragility curves of the 2018 Sulawesi-Palu tsunami

The 2018 Sulawesi-Palu tsunami curves are developed for confined masonry buildings with unreinforced clay brick from DB_Palu2018'. The computed and surveyed curves show a similar damage trend with a 90 % of buildings reaching or exceeding partial damage repairable (ds_1), 40 % partial damage unrepairable (ds_2) and 15 % complete damage (ds_3) when both flow depths reach 1.5 m (Fig. 15a,b). The fragility curves based on observation and simulation are similar enough to consider the computed curves as functions of the hydrodynamic features of the tsunami reliable (Fig. 15c,d). The building damage probabilities are presented for 2.5 m flow depth, 3 m/s flow velocity and 15 kN/m hydrodynamic force in Table 11.

https://doi.org/10.5194/nhess-2020-395
Preprint. Discussion started: 16 December 2020

Natural Hazards and Earth System Sciences
Discussions

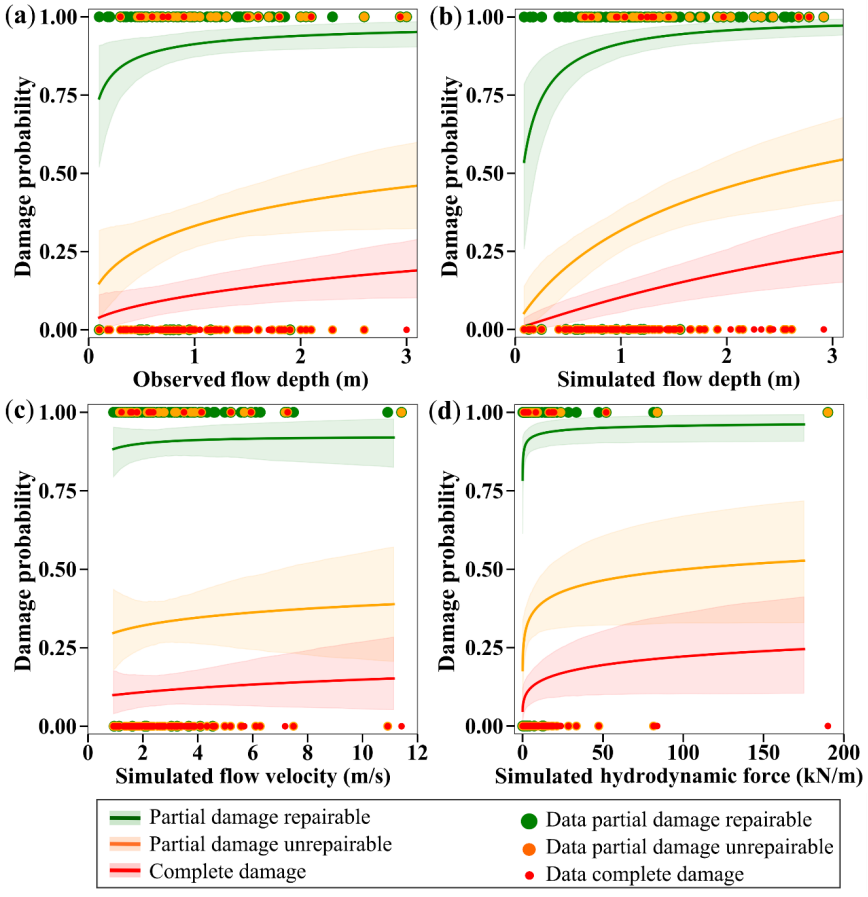

Figure 15. Best-estimate fragility curves, with their 90 % confidence intervals, as functions of (a) the observed flow depth, (b) the maximum simulated flow depth, (c) the maximum simulated flow velocity and the simulated hydrodynamic force for confined masonry-type buildings with unreinforced clay brick of DB_Palu2018' sustaining partial damage repairable (ds_1, green), partial damage unrepairable (ds_2, orange) and complete damage (ds_3, red) in Palu-City.

Table 11. Damage probabilities (ds_{1-3}) when the simulated flow depth, flow velocity and hydrodynamic force reach 2.5 m, 3 m/s and 15 kN/m respectively for confined masonry-type buildings with unreinforced clay brick (Paulik et al., 2019) (Fig. 15b-d) of DB_Palu2018'.

Damage state	Tsunami intensity measure	Building damage probability (%)
Partial repairable (ds_1)	2.5 m	96
	3 m/s	90
	15 kN/m	94
Partial unrepairable (ds_2)	2.5 m	50
	3 m/s	33
	15 kN/m	40
Complete (ds_3)	2.5 m	22

https://doi.org/10.5194/nhess-2020-395
Preprint. Discussion started: 16 December 2020

	3 m/s	11
	15 kN/m	15

5.3 Comparison between the 2018 and 2004 building fragility curves

In this section, the curves developed previously are compared with those realized for the 2004 IOT in Banda Aceh (Indonesia) and in Khao Lak/Phuket, Thailand (DB_Thailand2004). The fragility curves proposed by Koshimura et al., 2009a are based on a visual damage interpretation of remaining roofs in Banda Aceh using the pre and post-tsunami satellite data (IKONOS). Therefore, these curves are developed for mixed buildings devastated (low-rise wooden, timber-framed and non-engineered reinforced-concrete constructions (Koshimura et al., 2009a; Saatcioglu et al., 2006)) (Fig. 16a,b,c). The Sunda Strait and Sulawesi-Palu curves are presented for completely damaged/washed away confined masonry-type buildings and are functions of the simulated tsunami intensity. In Khao Lak/Phuket, the fragility curve is a function of the observed flow depth for collapsed reinforced-concrete infilled frames buildings (Foytong and Ruangrassamee, 2007; Rossetto et al., 2007; Ruangrassamee et al., 2006), as shown in Fig. 16a.

For 1-m flow depth, the percentage of buildings reaching complete damage is greater in Palu (10 %) than in Banda Aceh, Khao Lak/Phuket and the Sunda Strait, where less than 5 % of the structures sustain this damage state (Fig. 16a, Table 12). However, when the flow depth reaches 3 m, half of the buildings are destroyed in Banda Aceh against only one quarter in Palu-city and less than 20 % in Khao Lak/Phuket. We also note that the percentage of destructed buildings is higher in the Sunda Strait than in Khao Lak/Phuket above 4-m flow depth. However, the data points in Thailand are mostly ranging from 0 to 5 m and the 90 % confidence interval upon this value is constantly increasing with the flow depth. The flow velocity has a low impact on the damage probability below 1 m/s in Banda Aceh (< 1 %) (Fig. 16b, Table 12). Beyond this value, the percentage of damage becomes largely sensitive to the current velocity contrary to the Sunda Strait or Palu. As an example, when the flow velocity attains 6 m/s, only 25 % and 13 % of houses are demolished in Sunda Strait and Palu areas respectively in opposite to Banda Aceh, where the majority of constructions is completely damaged. Moreover, the building damage probability in Banda Aceh increases steeply with the flow velocity compared to Palu, where approximately 15 % of structures are destructed irrespective of the flow velocity, ranging from 1 to 10 m/s. The hydrodynamic force highly contributes to increasing probability of complete building damage in Banda Aceh and in the Sunda Strait. For example, the majority of constructions are devastated in Banda Aceh when the force reaches 25 kN/m while in Palu, only 17 % of buildings collapsed (Fig. 16c, Table 12). We also note the damage probability slightly increases with the hydrodynamic force of the Sulawesi-Palu tsunami; whether the tsunami load on buildings is 25 or 100 kN/m, around 20 % of buildings are completely damaged.

https://doi.org/10.5194/nhess-2020-395
Preprint. Discussion started: 16 December 2020

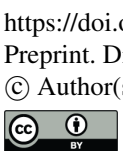

Natural Hazards and Earth System Sciences
Discussions

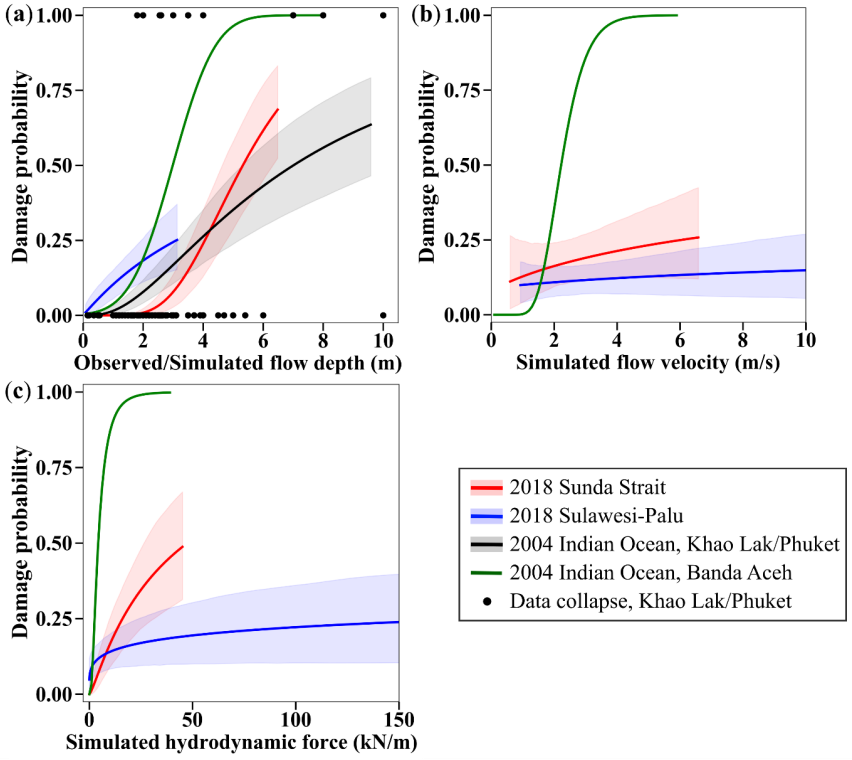

Figure 16. Best-estimate fragility curves for the 2018 Sunda Strait tsunami (red), 2018 Sulawesi-Palu tsunami (blue), 2004 Indian Ocean tsunami in Khao Lak/Phuket, Thailand (black) and Banda Aceh, Indonesia (Koshimura et al., 2009a) (green) as functions of (a) the observed/maximum simulated flow depth, (b) the maximum simulated flow velocity, and (c) the simulated hydrodynamic force. These fragility functions are developed only for completely damaged or washed away buildings with their 90 % confidence intervals.

Table 12. Damage probabilities of buildings completely damaged according to the intensity measures of the Sunda Strait, Palu, Khao Lak/Phuket and Banda Aceh (Koshimura et al., 2009a) tsunamis (Fig. 16a-c).

Tsunami intensity measure		Building damage probability (%)			
		Sunda Strait	Palu	Khao Lak/Phuket	Banda Aceh
Observed/Simulated flow depth (m)	1	< 1	10	< 1	4
	3	8	25	17	50
	6	62	-	43	99
Simulated flow velocity (m/s)	1	13	10	-	< 1
	3	19	11	-	85
	6	25	13	-	99
Simulated hydrodynamic force (kN/m)	25	35	17	-	99
	50	48	19	-	99
	100	-	22	-	-

https://doi.org/10.5194/nhess-2020-395
Preprint. Discussion started: 16 December 2020

Natural Hazards and Earth System Sciences
Discussions

6. Discussion

The curves comparison illustrates remarkably well the relationship between the 2004 Indian Ocean, the 2018 Sunda Strait and the 2018 Sulawesi-Palu tsunamis features, summarized in Table 13, and the structural performance of buildings.

505

Table 13. Features of the 2004 IOT in Banda Aceh (Indonesia) and Khao Lak/ Phuket (Thailand), the 2018 Sulawesi-Palu and the 2018 Sunda Strait tsunamis.

Tsunami event	IO Banda Aceh	IO Khao Lak/Phuket	Sulawesi-Palu	Sunda Strait
Source	seismic earthquake	seismic earthquake	non-seismic landslides	non-seismic landslide
Ground shaking	++	-	+	-
Liquefaction	+/-	-	++	-
Wave period	long (~40 min)	long (~40 min)	short (~3.5 min)	short (~7 min)
Construction material	mixed (reinforced concrete, timber…)	reinforced concrete	confined masonry	confined masonry and timber

The 2018 Sunda Strait tsunami and the 2004 IOT, in Thailand, are characterized by dominant wave periods of 7 min (Muhari et al., 2019) and 40 min (Peiris, 2006) respectively. Ground shaking or liquefaction episodes were not reported before the arrival of these tsunamis meaning tsunami load is the primary cause of building damage. Fragility curves represented in Fig. 16a showed the short wave period tsunami in the Sunda Strait is less damaging than the 2004 IOT below 5-m flow depth. For instance, around 17 % of buildings are completely damaged in Thailand against only 8 % in Sunda Strait area for 3-m flow depth (Table 12). On the other hand, the Sunda Strait structures reveal a better performance than the ones in Thailand beyond 5-m flow depth. However, as few data points are available for completely damaged buildings in Thailand, the curve reliability is insufficient to illustrate the building damage probability according to the flow depth.

Contrary to Thailand, strong ground shaking and few liquefaction episodes have been reported before the arrival of the 2004 IOT in the city of Banda Aceh, where the building damage has been substantial (Ghobarah et al., 2006; Koshimura et al., 2009a; Lavigne et al., 2009; Saatcioglu et al., 2006). Fragility curves as a function of the flow depth indicate that building resilience is higher in Thailand than in Banda Aceh (Fig. 16a). For example, 99 % and 43 % of buildings are completely damaged/washed away in Banda Aceh and Khao Lak/ Phuket respectively for 4-m flow depth. Therefore, due to prior ground shaking, the structures have been damaged before the arrival of the tsunami in Banda Aceh.

The 2018 Sulawesi earthquake (M_w= 7.5) also induced ground shaking leading to severe liquefaction episodes in Palu-City and the surrounding area. This event is characterized by short wave period just as the 2018 Sunda Strait tsunami, also triggered by a non-seismic source. The tsunami dominant wave periods are estimated to 3.5 min in Palu (Syamsidik et al., 2019a) and 7 min in the Sunda Strait (Muhari et al., 2019). Based on the flow depth, buildings affected by the Sulawesi-Palu tsunami were more susceptible to complete damage (Fig. 16a). For 3-m

https://doi.org/10.5194/nhess-2020-395
Preprint. Discussion started: 16 December 2020

flow depth, 25 % of buildings collapsed in Palu compared to 8 % in the Sunda Strait. On the other hand, according to the flow velocity and the hydrodynamic force of the tsunamis, the damage probability is higher in the Sunda Strait than in Palu (Fig. 16b,c). For 6 m/s flow velocity, 25 % and 13 % of buildings are completely damaged in Sunda Strait and Palu areas respectively. When the hydrodynamic force reaches 25 kN/m, around 35 % of constructions are destroyed in the Sunda Strait against 17 % only in Palu (Table 12). In addition, the damage ratio in Palu increases very less according to the flow velocity and the hydrodynamic force. Thereby, the tsunami load is not responsible for the main structural destruction as buildings were likely to be damaged before the arrival of the tsunami. According to Mas et al., 2020, ground shaking did not affect or only caused minor damage to buildings in Palu. Therefore, liquefaction episodes are mostly responsible for the building damage. Despite its non-seismic source, the Sulawesi-Palu tsunami causes a higher building damage probability up to 2-m flow depth, compared to the 2004 IOT in Banda Aceh characterized by a seismic source and ground shaking. As an example, 10 % of buildings are completely devastated in Palu against less than 5 % in Banda Aceh for 1-m flow depth (Table 12). In other words, in case of strong liquefaction, a non-seismic tsunami can be more damaging than a seismic one.

Through the 2004 Indian Ocean, the 2018 Sulawesi-Palu and the 2018 Sunda Strait tsunamis, we illustrate the impact of the wave period, ground shaking and liquefaction episodes on building performance. However, the effect due to floating debris on buildings and infrastructure is not considered in TUNAMI 2-layer. Debris carried by the tsunami flow represent a real threat for infrastructures (Ko et al., 2015). For instance, in Banda Aceh, due to the flat topography and the consequent hydrodynamic features of the Indian Ocean tsunami, heavy debris floating have been reported, which contributes to the destruction of the remaining buildings (Saatcioglu et al., 2006). In Thailand, buildings have also been impacted by floating debris (Ghobarah et al., 2006; Rossetto et al., 2007). Therefore, such impact should be included in numerical modelling in the future.

7. Conclusions

The tsunami intensity of the 2018 Sunda Strait and Sulawesi-Palu tsunamis are reproduced with TUNAMI two-layer model. Both tsunami inundation models are successfully validated based on the observed flow depth data at buildings. From the simulated tsunami hydrodynamic features and/or damaged building data, the fragility curves of the 2004 IOT in Khao Lak/Phuket (Thailand), 2018 Sunda Strait and 2018 Sulawesi-Palu tsunamis are developed according the construction material (confined masonry, reinforced concrete and timber). The reliability of the tsunami inundation models is demonstrated by the high similarity between surveyed and computed building fragility curves. Koshimura et al., 2009a developed tsunami curves in Banda Aceh, which are compared with the ones developed in this study for completely damaged/washed away buildings only. This comparison aims to highlight the characteristics of fragility curves for seismic or non-seismic tsunamis. The resulting curves show that a long wave period tsunami can further affect the resilience of buildings than a short wave period event. As an example, below 5-m flow depth, the 2018 Sunda Strait tsunami induces less damage than the 2004 IOT in Khao Lak/Phuket, Thailand, characterized by longer wave period. As none of these locations reported ground shaking or liquefaction episodes before the arrival of the tsunamis, the probability of damage is entirely controlled by the wave period. Ground shaking also influences building performance. Before the 2004 IOT, the city of Banda Aceh reported tremors in contrast to Khao Lak/Phuket, Thailand, where only the tsunami load is responsible for the structural destruction. Consequently, for the same tsunami event, most of the buildings are completely damaged

https://doi.org/10.5194/nhess-2020-395
Preprint. Discussion started: 16 December 2020

Natural Hazards and Earth System Sciences
Discussions

in Banda Aceh while less than half of them collapses in Khao Lak/Phuket for 6-m inundation depth. Moreover, it is clearly demonstrated that liquefaction events can increase building susceptibility to tsunami damage. Although Palu-Bay was hit by a non-seismic tsunami with short wave period, the buildings were previously affected by severe liquefaction episodes. Therefore, under 2-m flow depth, the building damage probability is higher in Palu than in Banda Aceh, affected by ground shaking and struck by the longer wave period of the 2004 IOT.

Appendix A. Regression coefficients for the fragility curves of the 2018 Sunda Strait, 2018 Sulawesi-Palu and 2004 Indian Ocean in Khao Lak/Phuket, Thailand.

Table A1. Regression coefficients of the observed and simulated Sunda Strait tsunami intensity measures based on DB_Sunda2018'

Tsunami intensity measure	Regression coefficients (best estimate, standard error)				
	θ_{01}	θ_{02}	θ_{03}	θ_{1}	$\theta_{2(class=Timber)}$
Observed flow depth	-0.29, 0.415	-1.99, 0.402	-4.52, 0.639	2.76, 0.408	2.08,0.416
Simulated flow depth	-0.26, 0.377	-1.69, 0.355	-4.03, 0.545	2.40, 0.346	1.96, 0.390
Simulated flow velocity	0.80, 0.300	0.14, 0.293	-1.17, 0.307	0.27, 0.276	1.40, 0.296
Simulated hydrodynamic force	-4.07, 1.016	-4.95, 1.058	-6.50, 1.116	0.61, 0.118	1.45, 0.311

Table A2. Regression coefficients of the observed flow and simulated Sulawesi-Palu tsunami intensity measures based on DB_Palu2018'.

Tsunami intensity measure	Regression coefficients (best estimate, standard error)			
	θ_{01}	θ_{02}	θ_{03}	θ_{1}
Observed flow depth	1.35, 0.160	-0.43, 0.118	-1.21, 0.149	0.30, 0.154
Simulated flow depth	1.37, 0.163	-0.47, 0.120	-1.27, 0.152	0.51, 0.163
Simulated flow velocity	1.21, 0.231	-0.53, 0.213	-1.31, 0.232	0.10, 0.191
Simulated hydrodynamic force	0.26, 0.591	-1.51, 0.605	-2.30, 0.616	0.13, 0.073

Table A3. Regression coefficients of the observed flow depth during the 2004 Indian Ocean tsunami in Khao Lak/Phuket (Thailand) based on DB_Thailand2004.

Tsunami intensity measure	Regression coefficients (best estimate, standard error)			
	θ_{01}	θ_{02}	θ_{03}	θ_{1}
Observed flow depth (m)	0.39, 0.212	-0.89, 0.207	-2.20, 0.254	1.13, 0.188

Code and data availability. Post-tsunami field surveys data are available from references cited in the text. The bathymetric and topographic data for the Sunda Strait area were provided by BATNAS and DEMNAS, Indonesia, respectively (http://tides.big.go.id/DEMNAS/index.html). The Agency for Geo-spatial Information (BIG), Indonesia provided the bathymetric and topographic data for Palu-Bay. The tidal gauge records were supplied by the Coastal Disaster Mitigation Division, Ministry of Marine Affairs and Fisheries, Jakarta, Indonesia. Spatial data in this study are depicted through QGIS software.

https://doi.org/10.5194/nhess-2020-395
Preprint. Discussion started: 16 December 2020

Author Contributions. FI, AS, KP, EL, II and FB designed and coordinated this research. AS, KP and EL performed the tsunami simulations and participated to the calibration of the inundation models in Palu-Bay and in the Sunda Strait. SS and RP contributed to the tsunami data collection in Sunda Strait and Palu areas, respectively. II developed the fragility functions through advanced statistical analysis. All authors contributed to the drafting of the manuscript.

Competing interest. The authors declare that they have no conflict of interest.

Acknowledgements. This research was funded and supported by the Japan Society for the Promotion of Science (JSPS) Grant-in-Aid for Young Scientists, the JSPS-NRCT Bilateral Research grant, the World Class Professor (WCP) Program 2018-2020 Promoted by Ministry of Education And Culture of Republic of Indonesia, the Pacific Consultants Co., Ltd., the Willis Research Network (WRN), the Tokio Marine & Nichido Fire Insurance Co., Ltd., the National Institute of Water and Atmospheric Research (Project: CARH2106), UKRI GCRF Urban Disaster Risk Hub, and GLADYS.

References

Aburaya, T. and Imamura, F.: The proposal of a tsunami run-up simulation using combined equivalent roughness, Annual Journal of Coastal Engineering, Japan Society of Civil Engineers, 49, 276–280, 2002.

AIDA, I.: Reliability of a tsunami source model derived from fault parameters., Journal of Physics of the Earth, 26(1), 57–73, doi:10.4294/jpe1952.26.57, 1978.

Ammon, C. J., Ji, C., Thio, H.-K., Robinson, D., Ni, S., Hjorleifsdottir, V., Kanamori, H., Lay, T., Das, S. and Helmberger, D.: Rupture process of the 2004 Sumatra-Andaman earthquake, Science, 308(5725), 1133–1139, doi:10.1126/science.1112260, 2005.

Arikawa, T., Muhari, A., Okumura, Y., Dohi, Y., Afriyanto, B., Sujatmiko, K. A. and Imamura, F.: Coastal subsidence induced several tsunamis during the 2018 Sulawesi earthquake, Journal of Disaster Research, 13, 1–3, doi:10.20965/jdr.2018.sc20181204, 2018.

Asian Disaster Preparedness Center: The economic impact of the 26 December 2004 earthquake and Indian Ocean tsunami in Thailand, , 21 [online] Available from: https://reliefweb.int/report/thailand/economic-impact-26-december-2004-earthquake-and-indian-ocean-tsunami-thailand, 2007.

Association of Southeast Asian Nations (ASEAN)-Coordinating Centre for Humanitarian Assistance on disaster: Situation update No. 12 M 7.4 earthquake and tsunami Sulawesi, Indonesia. [online] Available from: https://reliefweb.int/sites/reliefweb.int/files/resources/AHA-Situation_Update-no12-Sulawesi-EQ-rev.pdf, 2018.

Attary, N., Van de Lindt, J. W., Unnikrishnan, V. U., Barbosa, A. R. and Cox, D. T.: Methodology for development of physics-based tsunami fragilities, Journal of Structural Engineering, 143(5), 04016223, 2017.

Carvajal, M., Araya-Cornejo, C., Sepúlveda, I., Melnick, D. and Haase, J. S.: Nearly instantaneous tsunamis following the Mw 7.5 2018 Palu earthquake, Geophysical Research Letters, 46(10), 5117–5126, doi:10.1029/2019GL082578, 2019.

https://doi.org/10.5194/nhess-2020-395
Preprint. Discussion started: 16 December 2020

Chakrabarti, S.: Handbook of Offshore Engineering (2-volume set), Elsevier., 2005.

Day, S. J.: Volcanic tsunamis, in The Encyclopedia of Volcanoes, edited by H. Sigurdsson, B. Houghton, S. McNutt, H. Rymer, and J. Stix, pp. 993–1009, Elsevier., 2015.

Federal Emergency Management Agency (FEMA): Coastal construction manual, FEMA 55, Third Edition (FEMA 55), 296p., 2003.

Foytong, P. and Ruangrassamee, A.: Fragility curves of reinforced-concrete buildings damaged by a tsunami for tsunami risk analysis, in The Twentieth KKCNN Symposium on Civil Engineering, Jeju, Korea, pp. 4–5., 2007.

Frederik, M. C. G., Udrekh, Adhitama, R., Hananto, N. D., Asrafil, Sahabuddin, S., Irfan, M., Moefti, O., Putra, D. B. and Riyalda, B. F.: First results of a bathymetric survey of Palu Bay, Central Sulawesi, Indonesia following the tsunamigenic earthquake of 28 September 2018, Pure and Applied Geophysics, 176(8), 3277–3290, doi:10.1007/s00024-019-02280-7, 2019.

Ghobarah, A., Saatcioglu, M. and Nistor, I.: The impact of the 26 December 2004 earthquake and tsunami on structures and infrastructure, Engineering Structures, 28(2), 312–326, doi:10.1016/j.engstruct.2005.09.028, 2006.

Grezio, A., Babeyko, A., Baptista, M. A., Behrens, J., Costa, A., Davies, G., Geist, E. L., Glimsdal, S., González, F. I., Griffin, J., Harbitz, C. B., LeVeque, R. J., Lorito, S., Løvholt, F., Omira, R., Mueller, C., Paris, R., Parsons, T., Polet, J., Power, W., Selva, J., Sørensen, M. B. and Thio, H. K.: Probabilistic tsunami hazard analysis: multiple sources and global applications, Reviews of Geophysics, 55(4), 1158–1198, doi:10.1002/2017RG000579, 2017.

Grilli, S. T., Tappin, D. R., Carey, S., Watt, S. F. L., Ward, S. N., Grilli, A. R., Engwell, S. L., Zhang, C., Kirby, J. T., Schambach, L. and Muin, M.: Modelling of the tsunami from the December 22, 2018 lateral collapse of Anak Krakatau volcano in the Sunda Straits, Indonesia, Scientific Reports, 9(1), 1–13, doi:10.1038/s41598-019-48327-6, 2019.

Heidarzadeh, M., Muhari, A. and Wijanarto, A. B.: Insights on the source of the 28 September 2018 Sulawesi tsunami, Indonesia based on spectral analyses and numerical simulations, Pure and Applied Geophysics, 176(1), 25–43, doi:10.1007/s00024-018-2065-9, 2019.

Heidarzadeh, M., Ishibe, T., Sandanbata, O., Muhari, A. and Wijanarto, A. B.: Numerical modeling of the subaerial landslide source of the 22 December 2018 Anak Krakatoa volcanic tsunami, Indonesia, Ocean Engineering, 195, 106733, doi:10.1016/j.oceaneng.2019.106733, 2020.

Imamura, F.: Review of tsunami simulation with a finite difference method, Long-Wave Runup Models, 25–42, 1996.

Imamura, F. and Imteaz, M. A.: Long waves in two layers: governing equations and numerical model, Science of Tsunami Hazards, 13(1), 3–24, 1995.

Japan Society of Civil Engineers (JSCE): Tsunami assessment method for nuclear power plants in Japan, Japan Society of Civil Engineers Tokyo. [online] Available from: https://www.jsce.or.jp/committee/ceofnp/Tsunami/eng/JSCE_Tsunami_060519.pdf, 2002.

https://doi.org/10.5194/nhess-2020-395
Preprint. Discussion started: 16 December 2020

Ko, H. T. S., Cox, D. T., Riggs, H. R. and Naito, C. J.: Hydraulic experiments on impact forces from tsunami-driven debris, Journal of Waterway, Port, Coastal, and Ocean Engineering, 141(3), 04014043, doi:10.1061/(ASCE)WW.1943-5460.0000286, 2015.

Koshimura, S., Oie, T., Yanagisawa, H. and Imamura, F.: Developing fragility functions for tsunami damage estimation using numerical model and post-tsunami data from Banda Aceh, Indonesia, Coastal Engineering Journal, 51(3), 243–273, doi:10.1142/S0578563409002004, 2009a.

Koshimura, S., Namegaya, Y. and Yanagisawa, H.: Tsunami fragility - A new measure to identify tsunami damage, Journal of Disaster Research, 4(6), 479–488, doi:10.20965/jdr.2009.p0479, 2009b.

Kotani, M.: Tsunami run-up simulation and damage estimation using GIS, Pacific Coast Engineering, Japan Society of Civil Engineers (JSCE), 45, 356–360, 1998.

Krüger, F. and Ohrnberger, M.: Spatio-temporal source characteristics of the 26 December 2004 Sumatra earthquake as imaged by teleseismic broadband arrays, Geophysical Research Letters, 32(24), doi:10.1029/2005GL023939, 2005.

Lauterjung, J., Münch, U. and Rudloff, A.: The challenge of installing a tsunami early warning system in the vicinity of the Sunda Arc, Indonesia, Natural Hazards and Earth System Sciences, 10(4), 641–646, doi:10.5194/nhess-10-641-2010, 2010.

Lavigne, F., Paris, R., Grancher, D., Wassmer, P., Brunstein, D., Vautier, F., Leone, F., Flohic, F., De Coster, B., Gunawan, T., Gomez, C., Setiawan, A., Cahyadi, R. and Fachrizal: Reconstruction of tsunami inland propagation on December 26, 2004 in Banda Aceh, Indonesia, through field investigations, Pure and Applied Geophysics, 166(1–2), 259–281, doi:10.1007/s00024-008-0431-8, 2009.

Lay, T., Kanamori, H., Ammon, C. J., Nettles, M., Ward, S. N., Aster, R. C., Beck, S. L., Bilek, S. L., Brudzinski, M. R. and Butler, R.: The great Sumatra-Andaman earthquake of 26 December 2004, Science, 308(5725), 1127–1133, doi:10.1126/science.1112250, 2005.

Løvholt, F., Bungum, H., Harbitz, C. B., Glimsdal, S., Lindholm, C. D. and Pedersen, G.: Earthquake related tsunami hazard along the western coast of Thailand, Natural Hazards and Earth System Sciences, 6(6), 979–997, doi:10.5194/nhess-6-979-2006, 2006.

Macabuag, J., Rossetto, T. and Lloyd, T.: Sensitivity analyses of a framed structure under several tsunami design-guidance loading regimes, in 2nd European Conference on Earthquake Engineering and Seismology, Istanbul, Turkey. [online] Available from: http://www.eaee.org/Media/Default/2ECCES/2ecces_eaee/295.pdf, 2014.

Macabuag, J., Rossetto, T., Ioannou, I., Suppasri, A., Sugawara, D., Adriano, B., Imamura, F., Eames, I. and Koshimura, S.: A proposed methodology for deriving tsunami fragility functions for buildings using optimum intensity measures, Natural Hazards, 84(2), 1257–1285, doi:10.1007/s11069-016-2485-8, 2016.

Macías, J., Vázquez, J. T., Fernández-Salas, L. M., González-Vida, J. M., Bárcenas, P., Castro, M. J., Díaz-del-Río, V. and Alonso, B.: The Al-Borani submarine landslide and associated tsunami. A modelling approach, Marine Geology, 361, 79–95, doi:10.1016/j.margeo.2014.12.006, 2015.

https://doi.org/10.5194/nhess-2020-395
Preprint. Discussion started: 16 December 2020

Marfai, M. A., King, L., Singh, L. P., Mardiatno, D., Sartohadi, J., Hadmoko, D. S. and Dewi, A.: Natural hazards in Central Java Province, Indonesia: an overview, Environmental Geology, 56(2), 335–351, doi:10.1007/s00254-007-1169-9, 2008.

Mas, E., Koshimura, S., Suppasri, A., Matsuoka, M., Matsuyama, M., Yoshii, T., Jimenez, C., Yamazaki, F. and Imamura, F.: Developing tsunami fragility curves using remote sensing and survey data of the 2010 Chilean tsunami in Dichato, Natural Hazards and Earth System Sciences, 12(8), 2689–2697, 2012.

Mas, E., Paulik, R., Pakoksung, K., Adriano, B., Moya, L., Suppasri, A., Muhari, A., Khomarudin, R., Yokoya, N., Matsuoka, M. and Koshimura, S.: Characteristics of tsunami fragility functions developed using different sources of damage data from the 2018 Sulawesi earthquake and tsunami, Pure and Applied Geophysics, 177(6), 2437–2455, doi:10.1007/s00024-020-02501-4, 2020.

McCloskey, J., Antonioli, A., Piatanesi, A., Sieh, K., Steacy, S., Nalbant, S., Cocco, M., Giunchi, C., Huang, J. and Dunlop, P.: Tsunami threat in the Indian Ocean from a future megathrust earthquake west of Sumatra, Earth and Planetary Science Letters, 265(1–2), 61–81, doi:10.1016/j.epsl.2007.09.034, 2008.

Muhari, A., Imamura, F., Arikawa, T., Hakim, A. R. and Afriyanto, B.: Solving the puzzle of the September 2018 Palu, Indonesia, tsunami mystery: clues from the tsunami waveform and the initial field survey data, Journal of Disaster Research, 13(Scientific Communication), sc20181108, doi:10.20965/jdr.2018.sc20181108, 2018.

Muhari, A., Heidarzadeh, M., Susmoro, H., Nugroho, H. D., Kriswati, E., Supartoyo, Wijanarto, A. B., Imamura, F. and Arikawa, T.: The December 2018 Anak Krakatau Volcano tsunami as inferred from post-tsunami field Surveys and Spectral Analysis, Pure and Applied Geophysics, 176(12), 5219–5233, doi:10.1007/s00024-019-02358-2, 2019.

Murao, O. and Nakazato, H.: Development of fragility curves for buildings based on damage survey data in Sri Lanka after the 2004 Indian Ocean tsunami, Journal of Structural and Construction Engineering, 75(651), 1021–1027, doi:10.3130/aijs.75.1021, 2010.

Nalbant, S. S., Steacy, S., Sieh, K., Natawidjaja, D. and McCloskey, J.: Earthquake risk on the Sunda trench, Nature, 435(7043), 756–757, doi:10.1038/nature435756a, 2005.

National Agency for Disaster Management (BNPB): The Sunda Strait tsunami. [online] Available from: https://reliefweb.int/report/indonesia/indonesia-sunda-strait-tsunami-dg-echo-bnpb-ocha-ifrc-media-echo-daily-flash-23, 2018.

Omira, R., Dogan, G. G., Hidayat, R., Husrin, S., Prasetya, G., Annunziato, A., Proietti, C., Probst, P., Paparo, M. A., Wronna, M., Zaytsev, A., Pronin, P., Giniyatullin, A., Putra, P. S., Hartanto, D., Ginanjar, G., Kongko, W., Pelinovsky, E. and Yalciner, A. C.: The September 28th, 2018, tsunami in Palu-Sulawesi, Indonesia: a post-event field survey, Pure and Applied Geophysics, 176(4), 1379–1395, doi:10.1007/s00024-019-02145-z, 2019.

Otake, T., Chua, C. T., Suppasri, A. and Imamura, F.: Justification of possible casualty-reduction countermeasures based on global tsunami hazard assessment for tsunami-prone regions over the past 400 years, Journal of Disaster Research, 15(4), 490–502, doi:10.20965/jdr.2020.p0490, 2020.

https://doi.org/10.5194/nhess-2020-395
Preprint. Discussion started: 16 December 2020

Pakoksung, K., Suppasri, A. and Imamura, F.: Systematic evaluation of different infrastructure systems for tsunami defense in Sendai City, Geosciences, 8(5), 173, doi:10.3390/geosciences8050173, 2018.

Pakoksung, K., Suppasri, A., Imamura, F., Athanasius, C., Omang, A. and Muhari, A.: Simulation of the submarine landslide tsunami on 28 September 2018 in Palu Bay, Sulawesi Island, Indonesia, using a two-layer model, Pure and Applied Geophysics, 176(8), 3323–3350, doi:10.1007/s00024-019-02235-y, 2019.

Paris, A., Heinrich, P., Paris, R. and Abadie, S.: The December 22, 2018 Anak Krakatau, Indonesia, landslide and tsunami: preliminary modeling results, Pure and Applied Geophysics, 177(2), 571–590, doi:10.1007/s00024-019-02394-y, 2020.

Paulik, R., Gusman, A., Williams, J. H., Pratama, G. M., Lin, S., Prawirabhakti, A., Sulendra, K., Zachari, M. Y., Fortuna, Z. E. D., Layuk, N. B. P. and Suwarni, N. W. I.: Tsunami hazard and built environment damage observations from Palu City after the September 28 2018 Sulawesi earthquake and tsunami, Pure and Applied Geophysics, 176(8), 3305–3321, doi:10.1007/s00024-019-02254-9, 2019.

Peiris, N.: Vulnerability functions for tsunami loss estimation, in First European conference on earthquake engineering and seismology, Geneva, Switzerland, pp. 3–8., 2006.

Rastogi, B.: A historical account of the earthquakes and tsunamis in the Indian Ocean, in The Indian Ocean Tsunami, pp. 3–18, Taylor & Francis., 2007.

Reese, S., Cousins, W. J., Power, W. L., Palmer, N. G., Tejakusuma, I. G. and Nugrahadi, S.: Tsunami vulnerability of buildings and people in South Java? Field observations after the July 2006 Java tsunami, Natural Hazards and Earth System Sciences, 7(5), 573–589, doi:10.5194/nhess-7-573-2007, 2007.

Rossetto, T., Peiris, N., Pomonis, A., Wilkinson, S. M., Del Re, D., Koo, R. and Gallocher, S.: The Indian Ocean tsunami of December 26, 2004: observations in Sri Lanka and Thailand, Natural Hazards, 42(1), 105–124, doi:10.1007/s11069-006-9064-3, 2007.

Rossetto, T., Ioannou, I., Grant, D. and Maqsood, T.: Guidelines for the empirical vulnerability assessment, [online] Available from: https://discovery.ucl.ac.uk/id/eprint/1449624/1/Rossetto_ULN-MOD-Empirical-vulnerability-201411-v01.pdf, 2014.

Ruangrassamee, A., Yanagisawa, H., Foytong, P., Lukkunaprasit, P., Koshimura, S. and Imamura, F.: Investigation of tsunami-induced damage and fragility of buildings in Thailand after the December 2004 Indian Ocean tsunami, Earthquake Spectra, 22(3_suppl), 377–401, doi:10.1193/1.2208088, 2006.

Saatcioglu, M., Ghobarah, A. and Nistor, I.: Performance of structures in Indonesia during the December 2004 Great Sumatra earthquake and Indian Ocean tsunami, Earthquake Spectra, 22(3_suppl), 295–319, doi:10.1193/1.2209171, 2006.

Sassa, S. and Takagawa, T.: Liquefied gravity flow-induced tsunami: first evidence and comparison from the 2018 Indonesia Sulawesi earthquake and tsunami disasters, Landslides, 16(1), 195–200, doi:10.1007/s10346-018-1114-x, 2019.

Sumer, B. M., Ansal, A., Cetin, K. O., Damgaard, J., Gunbak, A. R., Hansen, N.-E. O., Sawicki, A., Synolakis, C.

https://doi.org/10.5194/nhess-2020-395
Preprint. Discussion started: 16 December 2020

E., Yalciner, A. C., Yuksel, Y. and Zen, K.: Earthquake-induced liquefaction around marine structures, Journal of Waterway, Port, Coastal, and Ocean Engineering, 133(1), 55–82, doi:10.1061/(ASCE)0733-950X(2007)133:1(55), 2007.

Suppasri, A., Koshimura, S. and Imamura, F.: Developing tsunami fragility curves based on the satellite remote sensing and the numerical modeling of the 2004 Indian Ocean tsunami in Thailand, Natural Hazards and Earth System Sciences, 11(1), 173–189, doi:10.5194/nhess-11-173-2011, 2011.

Suppasri, A., Mas, E., Koshimura, S., Imai, K., Harada, K. and Imamura, F.: Developing tsunami fragility curves from the surveyed data of the 2011 Great East Japan tsunami in Sendai and Ishinomaki Plains, Coastal Engineering Journal, 54(1), 1250008-1-1250008–16, doi:10.1142/S0578563412500088, 2012.

Suppasri, A., Mas, E., Charvet, I., Gunasekera, R., Imai, K., Fukutani, Y., Abe, Y. and Imamura, F.: Building damage characteristics based on surveyed data and fragility curves of the 2011 Great East Japan tsunami, Natural Hazards, 66(2), 319–341, doi:10.1007/s11069-012-0487-8, 2013.

Suppasri, A., Charvet, I., Imai, K. and Imamura, F.: Fragility curves based on data from the 2011 Tohoku-oki tsunami in Ishinomaki city, with discussion of parameters influencing building damage, Earthquake Spectra, 31(2), 841–868, 2015.

Suppasri, A., Syamsidik, Pakoksung, K., Latcharote, P., Miyamoto, R. and Imamura, F.: Fragility functions of buildings under only tsunami load in Indonesia : a case study of the 2018 Sunda Strait tsunami, in 17th World Conference on Earthquake Engineering, 17WCEE, Sendai, Japan., 2020.

Sutikno, S.: Earthquake disaster of Yogyakarta and Central Java, and disaster reduction, Indonesia, Forum Geografi, 21(1), 1–16, doi:10.23917/forgeo.v21i1.1823, 2016.

Syamsidik, Benazir, Umar, M., Margaglio, G. and Fitrayansyah, A.: Post-tsunami survey of the 28 September 2018 tsunami near Palu Bay in Central Sulawesi, Indonesia: impacts and challenges to coastal communities, International Journal of Disaster Risk Reduction, 38, 101229, doi:10.1016/j.ijdrr.2019.101229, 2019a.

Syamsidik, S., Benazir, B. and Luthfi, M.: Tsunami flow depths, building damages, and tsunami boulders measured from the December 22, 2018 Sunda Strait tsunami around Western Java and Southern Lampung of Indonesia, Mendeley Data [online] Available from: https://data.mendeley.com/datasets/yyyvmxh8vg/1, 2019b.

Syamsidik, S., Luthfi, M., Suppasri, A. and Comfort, L. K.: The 22 December 2018 Mount Anak Krakatau volcanogenic tsunami on Sunda Strait coasts, Indonesia: tsunami and damage characteristics, Natural Hazards and Earth System Sciences, 20(2), 549–565, doi:10.5194/nhess-20-549-2020, 2020.

Ward, S. N.: Landslide tsunami, Journal of Geophysical Research: Solid Earth, 106(B6), 11201–11215, doi:10.1029/2000JB900450, 2001.